

JGR Solid Earth

RESEARCH ARTICLE

10.1029/2018JB017200

Special Section:

Physical Properties of Rocks, Friction and Fracturing: the Walsh Volume

Key Points:

- Electrokinetic transport through inhomogeneously charged 3-D nanoporous rocks is investigated with pores fully screened via EDL
- Significant underestimation of local electric potential and electrokinetic transport mechanisms are revealed when assuming homogeneous surface charge
- Inhomogeneous surface charge causes higher electrical conductivity, electroosmotic permeability, and tortuosity compared with a prescribed homogeneous charge of nanoporous rocks

Correspondence to:

M. Wang,
mrwang@tsinghua.edu.cn

Citation:

Alizadeh, A., Jin, X., & Wang, M. (2019). Pore-scale study of ion transport mechanisms in inhomogeneously charged nanoporous rocks: Impacts of interface properties on macroscopic transport. *Journal of Geophysical Research: Solid Earth*, 124. <https://doi.org/10.1029/2018JB017200>

Received 17 DEC 2018

Accepted 19 APR 2019

Accepted article online 25 APR 2019

Pore-scale Study of Ion Transport Mechanisms in Inhomogeneously Charged Nanoporous Rocks: Impacts of Interface Properties on Macroscopic Transport

Amer Alizadeh¹ , Xu Jin², and Moran Wang¹ 

¹Department of Engineering Mechanics and CNMM, Tsinghua University, Beijing, China, ²National Energy Tight Oil and Gas Research Centre, Petroleum Geology Research and Laboratory Center, Research Institute of Petroleum Exploration and Development (RIPEDE) PetroChina, Beijing, China

Abstract The electrokinetic transport mechanisms of multispecies ions through 3-D nanoporous rocks with chemical reaction at the solid-aqueous solution interfaces are investigated. We systematically study the multiphysics transport phenomena by considering either inhomogeneous (local surface charge based on local pH and ion concentrations) or prescribed homogeneous surface charge at solid-aqueous solution interface while the pores are screened via electric double layers. We develop a lattice Boltzmann numerical framework to solve the set of governing equations (Poisson-Nernst-Planck plus Navier–Stokes). Our modeling results reveal that the averaged local electric potential of the nanoporous rock is significantly underestimated (about 83%) when a homogeneous surface charge is prescribed based on the bulk solution properties. It is shown that increasing the porosity of the nanoporous media considerably increases the absolute values and inhomogeneity of the surface charge, which means that while the electric double layers screened the pores, increasing the porosity enhances the ion selectivity of the porous medium. When the scenario with inhomogeneous charge is taken into account, the predicted electroosmotic permeability and tortuosity are higher in comparison with the prescribed homogeneous case. Moreover, we have studied the electrostatic tortuosity, coupling coefficient, and the effective excess charge density of the nanoporous rocks. The results demonstrate that ignoring the inhomogeneity of surface charges may cause erroneous prediction of the ion transport through porous rocks with chemically active surfaces.

Plain Language Summary How can we study the subsurface geological properties? How can we understand the contaminant deposition rate at underground? How can we provide a better understanding of the diffusion and dispersion phenomena in tight rocks? To answer these questions, one needs to consider the transport of multispecies ions through the complex geometries like unstructured porous media. However, these transport mechanisms are highly coupled multiphysicochemical phenomena, which are influenced by the local properties of the solid-aqueous solution interface such as locally acquired surface charge. In the present contribution, we scale down our vision into the pore-scale to understand what is happening inside these complex mazes when we apply external body forces (i.e., applied an electric field and pressure gradient). The modeling results revealed several substantial facts that a great underestimation for the local electric potential of the porous rocks will happen when someone ignores the locally acquired surface charge due to local solution properties. In addition, it has been shown that the movement of the ions and water flow should be more tortuous when we consider the electric charge inhomogeneity compared with a prescribed homogenous surface charge. Measuring the electrical and streaming conductivity of the nanoporous rocks, which play a key role in studying the underground geological properties, demonstrates higher amounts for inhomogeneously surface charge.

1. Introduction

Charged nanoporous media and ion-selective nanochannels have attracted considerable interests in recent decades owing to their ever-increasing applications from geophysics and environment (Dykstra et al., 2017; Johnson et al., 1996; Ko et al., 2012; Lacoste et al., 2009; Li et al., 2013; Massimo et al., 2018; Muhammad & Massimo, 2015, 2017; Nikonenko et al., 2014; Revil, Pezard, & Glover, 1999; Revil, Schwaeger, et al., 1999; Schultz, 1997; S. Song et al., 2004; Sun et al., 2001; Vane & Zang, 1997) to energy conversion (D. K. Kim,

Duan, et al., 2010), water desalination (Nikonenko et al., 2014; Sung Jae et al., 2010; Suss et al., 2012), and even biophysics (Bhadra et al., 2016; Hotta et al., 2012; Ko et al., 2012). A crucial common factor among these applications is the presence of ionic transport through structured or unstructured materials with charged solid-aqueous solution interfaces. Focusing on the geological and environmental applications, the transport of colloidal particles in subsurface aqueous environments is of great importance for studying the contaminants transport and adsorption on to colloids (Elimelech, 1992; Molnar et al., 2015; Tobiason, 1989). It was argued that there must be surface charge inhomogeneity at both microscopic (pore-scale) and macroscopic (field-scale) scale to explain the deposition rate (Kretzschmar et al., 1999; Ryan & Elimelech, 1996; L. F. Song et al., 1994). On the other hand, better understanding of the ionic transport through complex geometries with inhomogeneously charged surfaces could improve our knowledge of the geological measurements (i.e., streaming potential [Andre Revil & Leroy, 2004; Revil, Pezard, & Glover, 1999; Revil, Schwaeger, et al., 1999]), solute transport for concrete pores (Appelo, 2017; Yang & Wang, 2018a), diffusion (Yang & Wang, 2018b) and dispersion in porous media (Muniruzzaman et al., 2014; Rolle et al., 2013), reactive transport (Alt-Epping et al., 2015; Muniruzzaman & Rolle, 2016; Steefel & Maher, 2009; Zhang & Wan, 2015), salt removal and electro-diffusion of shale layer [Andre Revil & Leroy, 2004], and underground water quality (Muniruzzaman & Rolle, 2016).

The macroscopic transport in charged microporous media has been well studied by volume-averaging the local Nernst-Planck and Navier-Stokes equations (Revil & Linde, 2006) and considering the Donnan equilibria. Revil and Linde generalized the Teorell Meyer Sievers model to obtain the local concentrations of the multispecies ions in a charged porous media. Yet it is well understood that variations of local charges could arise from the chemical reactions of the solid surface (i.e., silica) with the aqueous solution as well as from mineralogical or structural inhomogeneities in rocks. The local solution pH, temperature, and ion concentration (thermo-chemical properties) determine the final acquired surface charge (Alizadeh & Wang, 2018; Revil, Pezard, & Glover, 1999). Modeling the electrokinetic transport phenomena through electrically charged nanoporous media is challenging due to three main difficulties: first, the complex geometry of the porous media, which brings such a great complexity to the governing equations; second, obtaining the local surface charge based on the local solution thermo-chemical properties, which posture as the main bottleneck; and finally, the thickness of the electric double layer (EDL) within the pores of the porous media. The thickness of the EDL in comparison with the representative pore size of the porous media has a key role in electrokinetic transport phenomena. For instance, when the thickness of the EDL is comparative with the pore size (or even larger), the whole pore space would be electrically charged. This means that the ion selectivity of the nanoporous media is significantly enhanced. This phenomenon is recognized as the ion concentration polarization, which happens at the intersection of the microfluidic and nanofluidic channels (Pu et al., 2004) or at the vicinity of the ion selective membranes like Nafion (S. J. Kim, Ko, et al., 2010). However, the conventional theories, which lied on the Helmholtz-Smoluchowski equation, failed to predict the behavior of the nanoporous media for when the pores are screened via the EDLs. For sake of simplicity, the previous works tried to model ion transport through homogeneously charged nanotubes and nanochannels (Catalano et al., 2016; Fair & Osterle, 1971; Gross & Osterle, 1968; Peters et al., 2016; Wang, Kang, & Ben-Naim, 2010). Moreover, except a few studies, which relaxed the assumption related to the thickness of the EDL (Alizadeh et al., 2017; Fair & Osterle, 1971; Gross & Osterle, 1968; Liu et al., 2010; Peters et al., 2016), the majority of the literatures investigated the ion transport under the assumption of thin double-layer thickness; $\kappa\delta \gg 1$, where $\kappa = \lambda^{-1}$ and δ denote the reverse of Debye length

$$\lambda = \sqrt{\frac{\epsilon_0 \epsilon_r k_B T}{e^2 \sum_{i=1}^4 n_{i,0}}} \quad (1)$$

and the average radius or height of the nanopores, respectively (Burgreen & Nakache, 1964; Overbeek & Wijga, 1946; Rice & Whitehead, 1965; Zhang & Wang, 2017). In this relation, ϵ_0 [$\text{CV}^{-1}\text{m}^{-1}$] denotes the vacuum electrical permittivity, ϵ_r denotes the relative dielectric permittivity of the solution to the vacuum, k_B [JK^{-1}] denotes the Boltzmann constant, e [C] denotes the elementary charge of the electron, $n_{i,0}$ [m^{-3}] denotes the number density of the bulk ions, and T [K] denotes the absolute temperature of the solution. The assumption of the thin electrical double layer lets us use the electroosmotic velocity at the edge of the diffuse layer, and as a result, one can ignore the presence of the EDL. This assumption justifies the

employing of the Poisson-Boltzmann equation instead of the complex advection–diffusion (Nernst-Planck) equation. Only a few studies tried to tackle the electrokinetic transport through the porous media under the thick double-layer conditions (e.g., Andre Revil & Leroy, 2004; Galama et al., 2013; Revil & Linde, 2006; Revil et al., 2007).

Despite the aforementioned attempts, one can deduce that two main bottlenecks have not been tackled yet: taking into account the effects of the microstructure of real nanoporous media on the electrokinetic transport mechanisms and the local surface charge in the pores due to the variation of local pH and ion concentration. For understanding the physics underlying ion transport mechanisms through the charged nanoporous media, one has to solve the coupled Poisson, Nernst-Planck, and Navier–Stokes equations within a randomly generated porous medium. By utilizing a randomly generated porous medium, M. Wang and Chen (2007) investigated the electro-osmosis in a homogeneously charged microporous medium. Recently Zhang and Wang (2017) studied the ion transport through the inhomogeneously charged random porous medium by the aid of a simple 1-pK model (de Lima et al., 2008) for very thin EDLs ($\kappa\delta \gg 1$). In their work, the effect of the thin EDL has been introduced to the hydrodynamic equations by considering a slip velocity based on the Helmholtz-Smoluchowski classical equation (Hunter, 1981).

In this paper, we conduct a pore-scale study of the nonlinear electrokinetic transport phenomena for 3-D randomly generated nanoporous rocks, which acquire local surface charge due to chemical adsorption of the ions. Regarding the local surface charge, a representative bulk layer (RBL) model (Alizadeh & Wang, 2018) has been recently introduced to take into account not only the effects of the EDLs interaction (overlapped EDLs regime) but *also* the complex geometry of the randomly generated nanoporous rocks. Introducing the obtained local zeta potential to the Poisson's equation coupled with the Nernst-Planck and Navier–Stokes, equations enables us to study the electroosmotic permeability and tortuosity for inhomogeneously charged nanoporous media with overlapped EDLs. It is noteworthy that, although in the present contribution, we assume that the nanoporous media is made of pure silica (i.e., uniform surface complexation), the proposed numerical framework can be simply extended to model a porous media with a heterogeneous distribution of materials. In terms of the electrokinetic conductivity of the nanoporous media, we obtained the total streaming and electrical conductance of the nanoporous media as a function of the porosity and compared with when the rocks are assumed to be homogeneously charged.

2. Problem Definition

A porous medium is naturally made of randomly distributed pores and phases. The shape and position, as well as the pore size distribution, would be different in different samples. To approach a close to reality investigation of the ion transport through nanoporous media, in this contribution, 3-D nanoporous media are generated by the random generation growth method (instead of the structured porous medium; M. Wang & Chen, 2007; Moran Wang et al., 2007), which characterize the structure of porous media statistically. Although utilizing the 3-D nanoporous media will bring complexity to our calculation, however, this is an inevitable consequence of studying close to reality ion transport mechanisms through nanoporous media. On the other hand, solving the coupled governing equations in these 3-D unstructured porous media is the main uniqueness of the present contribution.

In this study, we take nanoporous media with dimensions Length $\equiv L = 1.5$ [μm], Height $\equiv H = 0.5$ [μm], and Width $\equiv W = 0.5$ (μm ; Figure 1). It is assumed that the nanoporous media are made of silica (Chua et al., 2015), which able to possess electric charge due to the chemical interaction with the aqueous solution at the vicinity of the solid-aqueous solution interfaces. The ionic fluxes and fluid flow through the nanoporous media are triggered by applying an external pressure gradient and electric field. The inlet of the nanoporous media is subjected to the well-mixed solution in which the electro-neutrality at inlet enforces $C_{K^+} = C_{KCl} + C_{KOH}$, $C_{Cl^-} = C_{HCl} + C_{KCl}$, $C_{H^+} = C_{HCl}$, and $C_{OH^-} = C_{KOH}$. In order to ensure that the EDLs are statistically overlapped in pore spaces, the concentration of the background solution is set to $C_{KCl} = 0.01$ [mM]. It is assumed that the diffusion coefficients of the ions, kinematic viscosity, and solution temperature are constant everywhere in the nanoporous media (Samson et al., 2003). The vacuum dielectric permittivity and the ratio of the electrolyte solution permittivity to the vacuum permittivity are defined in Table 1. For the electrically driven part of the ionic fluxes and fluid flow (electroosmotic flow), we apply an external

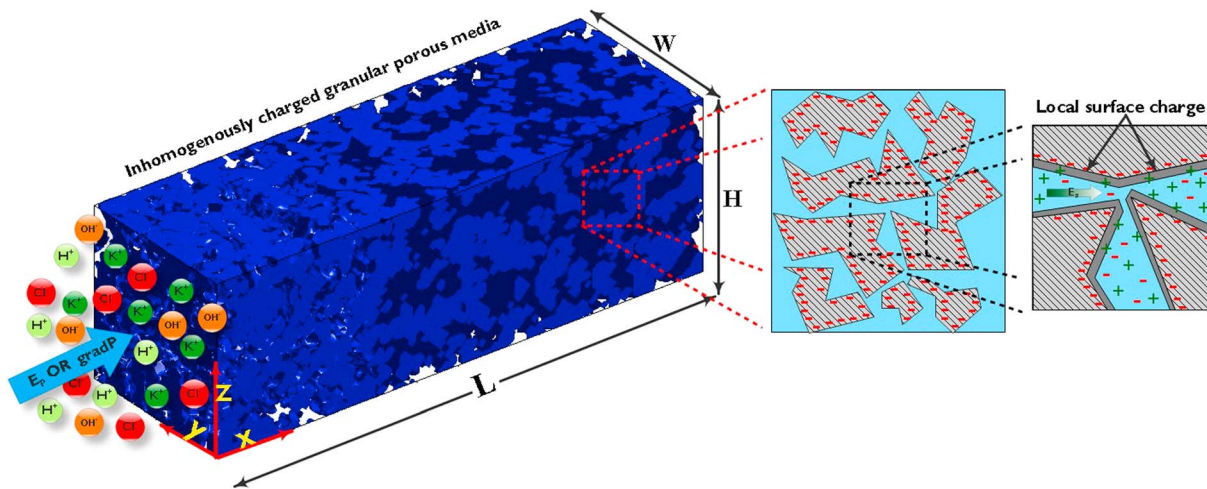


Figure 1. Schematic illustration of the nanoporous medium which is subjected to the multispecies ions (H^+ , OH^- , K^+ , Cl^-) at the inlet. The applied pressure gradient (∇p) and external electric potential field (E_p) impose ionic fluxes and fluid flow through the nanoporous medium. The local surface charge on the solid-aqueous solution interface is considered as a function of the local solution pH and ion concentration.

electric field. We apply a pressure gradient to the porous media to generate the pressure-driven flow. Table 1 presents the physicochemical parameters and their values.

We considered four porosities, $\epsilon = 0.3, 0.4, 0.5,$ and 0.6 , to investigate the effect of pore size on the ion transport mechanisms (Figure 2). The porosity of the randomly generated porous media is controlled by QSGS (Moran Wang et al., 2007). Note that we set the same dimensions for the nanoporous media with different porosities. In order to guarantee to have the overlapping regime of the EDLs in our nanoporous media, the characteristic lengths of the pores are determined to check if the pores are screened via the EDLs. In other words, for a prescribed ionic strength, one can manipulate the EDL interaction by the characteristic length of the pore size. Following the determination method of pore size in three orthogonal directions (Yanuka et al., 1986), the characteristic pore sizes for the aforementioned porosities are obtained as $d_{\epsilon=0.3} = 4.032$ [nm], $d_{\epsilon=0.4} = 12.4$ [nm], $d_{\epsilon=0.5} = 24.8$ [nm], and $d_{\epsilon=0.6} = 44.19$ [nm]. As a consequence, by considering the definition of the Debye length (Equation (1)), the ratio of the characteristic pore sizes to the characteristic length of the EDL, namely, Debye length, would be $\kappa d_{\epsilon=0.3} = 0.137$, $\kappa d_{\epsilon=0.4} = 0.42$, $\kappa d_{\epsilon=0.5} = 0.85$, and $\kappa d_{\epsilon=0.6} = 1.51$. Thus, for all nanoporous media, one can guarantee that the pores are fully screened by the electrical double layers (Zhang & Wang, 2017).

3. Mathematical Model and Numerical Methods

The classical electrokinetic transport theories are linear due to assuming a constant zeta potential and thin double layers, which result in the absence of EDL interaction. Under these conditions, the slip velocity at the edge of the diffuse layer is given by the classical Helmholtz-Smoluchowski equation

$$U_{HS} = -\frac{\epsilon_r \epsilon_0 \zeta E_p}{\eta} \quad (2)$$

where U_{HS} , ζ , E_p , and η represent the Helmholtz-Smoluchowski velocity, the zeta potential, the external electric field, and the dynamic viscosity of the solution, respectively. However, these assumptions essentially ignore the possible electro-chemo-mechanical transport phenomena in real applications since the assumption of constant zeta potential or thin double layers may fail in such complex geometries like porous structures. Thus, in order to take into account the possible multiphysical transport mechanisms in the porous media, the coupled Poisson, Nernst-Planck, and Navier-Stokes equations should be solved while the surface charges

Table 1
The Physicochemical Parameters and Their Values

Parameters	Value
D_{K^+}	$1.95 \times 10^{-9} [\text{m}^2 \text{s}^{-1}]$
D_{Cl^-}	$2.03 \times 10^{-9} [\text{m}^2 \text{s}^{-1}]$
D_{OH^-}	$5.27 \times 10^{-9} [\text{m}^2 \text{s}^{-1}]$
D_{H^+}	$9.31 \times 10^{-9} [\text{m}^2 \text{s}^{-1}]$
C_{KCl}	0.01 [mM]
ν	$8.89 \times 10^{-7} [\text{m}^2 \text{s}^{-1}]$
T	293.15 [K]
ϵ_0	$8.854 \times 10^{-12} [\text{CV}^{-1} \text{m}^{-1}]$
ϵ_r	78.54
E_p	$10^4 [\text{Vm}^{-1}]$
∇p	$41.6 \times 10^6 [\text{Pam}^{-1}]$

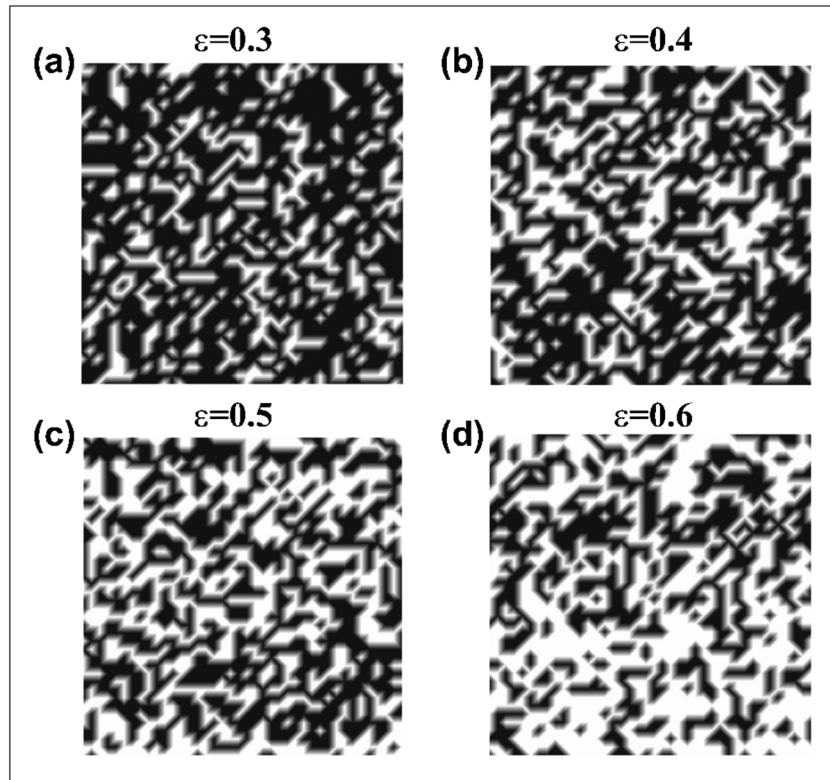


Figure 2. The slices of the 3-D randomly generated nanoporous media with porosities (a) $\varepsilon = 0.3$, (b) $\varepsilon = 0.4$, (c) $\varepsilon = 0.5$, and (d) $\varepsilon = 0.6$ on the y - z plane. The black color represents the solid and white one the voids of the porous media. The nanoporous media are generated via the random generation growth (RGG) method proposed by Wang et al. (Moran Wang et al., 2007) with $c_d = 0.08$.

on the solid-aqueous solution interfaces are determined based on the local solution properties in the pores. To obtain the local surface charge, we employ the recently developed comprehensive approach, so-called RBL model (Alizadeh & Wang, 2018), through which one can figure out the local surface charge based on the (I) local solution properties and (II) the impact of the structure of the porous media. In this section, we will present the governing equations, which are solved numerically by the coupled lattice Boltzmann methods.

3.1. Fluid Flow

In the modeled nanoporous rocks, the fluid flow is governed by the mass balance (under the assumption of the rigid solid skeleton) and the Navier–Stokes equations (Dutta & Beskok, 2001; D Li, 2004)

$$\frac{\partial \rho}{\partial t} + \nabla \cdot (\rho \mathbf{u}) = 0, \quad (3)$$

$$\frac{\partial (\rho \mathbf{u})}{\partial t} + \mathbf{u} \cdot \nabla (\rho \mathbf{u}) = -\nabla p + \nabla \cdot (\nu \nabla (\rho \mathbf{u})) + \mathbf{F}, \quad (4)$$

where ρ [kgm^{-3}] is the density of the electrolyte, \mathbf{u} [ms^{-1}] is the vector of flow velocity, t [s] is the time, p [Pa] is the fluid pressure, ν [m^2s^{-1}] is the kinematic viscosity, and \mathbf{F} [Nm^{-3}] is the body force density, which includes the implemented body forces such as electric force. Equations (3) and (4) are subjected to the non-slip boundary conditions at the solid–liquid interfaces ($\mathbf{u}_s = 0$), where \mathbf{u}_s denotes the velocity vector on the solid surface. For the inlet and outlet boundary conditions, we assume a constant pressure at either side to impose a pressure gradient. To solve the NS equations (Equations (3) and (4)), the lattice Boltzmann method as a novel solver for the partial differential equation is utilized. In this method, the multiphysical parameters (i.e., density, fluid flow velocity, electric potential, and ion concentration) are obtained by defining discretized distribution functions in 1-D, 2-D, or 3-D lattice systems. In the present contribution, we employ the

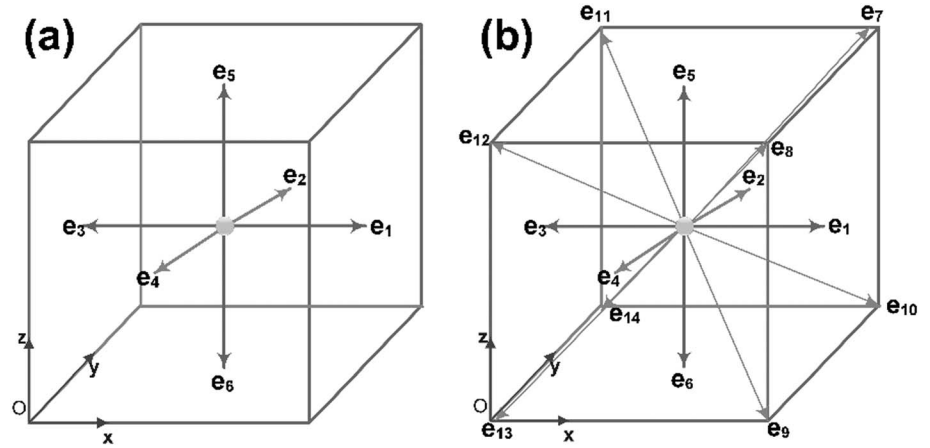


Figure 3. The schematic illustration of (a) D3Q7 and (b) D3Q15 discretized velocity in lattice Boltzmann models.

3-D lattice Boltzmann model with D3Q15 lattice system (Figure 3b). In order to avoid losing the main purpose of this study, we have not presented the details of the numerical algorithm since they are discussed in details elsewhere (Wang, Kang, Viswanathan, & Robinson, 2010).

3.2. Multispecies Ion Transport

The ion transport is governed by the mass conservation equation, which includes the advection–diffusion with an electrochemical migration source term as (Wang & Kang, 2010)

$$\frac{\partial C_i}{\partial t} + \nabla \cdot \mathbf{J}_i = 0, \quad (5)$$

where C_i represents the i th ion concentration and \mathbf{J}_i represents the species flux which consists of advection and diffusion terms (Lichtner, 1994; Wang & Kang, 2010)

$$\mathbf{J}_i = - \left(\frac{e z_i D_i}{k_B T} \right) C_i \nabla \Psi - D_i (\nabla C_i) + C_i \mathbf{u}, \quad (6)$$

where the first term on the right-hand side represents the electrochemical migration ($\Psi = \psi + \phi$, with Ψ , ψ , and ϕ denoting the total electric potential, the local electric potential due to the presence of EDLs, and externally applied electric potential $E_p = -\nabla \phi$, respectively) and the second term is the ion diffusion, and the last term advective transport. In Equation (6), e , z_i , D_i , k_B , and T are the absolute charge of the electron, valence number for i th ion, diffusion coefficient for i th ion, Boltzmann constant, and the absolute temperature, respectively (Li, 2004). By introducing Equation (6) into Equation (5) and considering isothermal electrolyte solution, the electrodynamic transport equation would be as (Lichtner, 1994)

$$\frac{\partial C_i}{\partial t} + \mathbf{u} \cdot \nabla C_i = D_i \nabla^2 C_i + \frac{e z_i D_i}{k_B T} \nabla \cdot (C_i \nabla \Psi), \quad (7)$$

where for solid-aqueous solution interfaces $\mathbf{J}_i = 0$, for inlet and outlet $C_i = n_{i,0}$ and $\partial C_i / \partial x = 0$, respectively. By employing a D3Q7 lattice system (Figure 3a), a lattice Boltzmann scheme has been proposed for the Nernst-Planck equations (Wang & Kang, 2010; Yoshida et al., 2014) in which all the contributions to the ionic fluxes are integrated into the collision operator and there would not be any source term. As a result, one can simply present the lattice Boltzmann evolution equation as (Yoshida et al., 2014)

$$h_i(\mathbf{X} + \mathbf{e}_i \delta_{t,h}, t + \delta_{t,h}) - h_i(\mathbf{X}, t) = - \left(\frac{1}{\tau_h} \right) [h_i(\mathbf{X}, t) - h_i^{\text{eq}}(\mathbf{X}, t)], \quad (8)$$

where h_i is the ionic distribution function, \mathbf{X} is the position vector, \mathbf{e}_i is the microscopic velocity vector of the particles in the D3Q7 model (Figure 3a), and $\delta_{t,h}$ is the time step and here is equal to 1. τ_h represents the dimensionless relaxation time which is defined as (Yoshida et al., 2014)

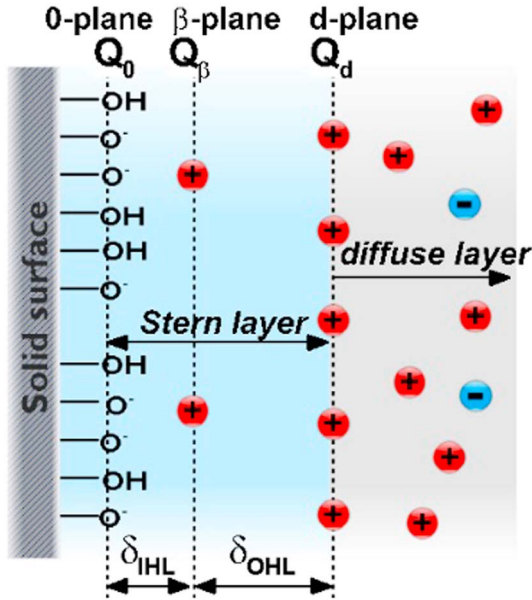


Figure 4. The electrical triple-layer model at the solid-aqueous solution interface. The electrical triple-layer model consists of three 0-, β -, and d - planes. The surface charge is represented by the Q_0 , and the zeta potential is obtained as ψ_d (Moran Wang & Revil, 2010).

could satisfy the zero ionic fluxes for solid surfaces (Yoshida et al., 2014). Thus, for the unknown distribution functions (h_i) on the solid surfaces, we have (Yoshida et al., 2014)

$$h_i^\alpha(\mathbf{X} + \mathbf{e}_i \delta_{t,h}, t + \delta_{t,h}) = h_i^\beta(\mathbf{X} + \mathbf{e}_i \delta_{t,h}, t), \quad (13)$$

where h_i^α denotes the unknown distribution functions and $\mathbf{e}_\alpha = -\mathbf{e}_\beta$. Here α and β denote the direction of the unknown distribution function and the bounce-back direction of α , which has known distribution function, respectively. For instance, in D3Q15 (Figure 3b), if $\mathbf{e}_{\alpha=11}$ represents an unknown direction for h_i^α , the $\mathbf{e}_{\beta=9}$ denotes the known direction of the distribution function h_i^β .

3.3. Local Electric Potential Field and Surface Complexation Reactions

The presence of the polarized solution at the vicinity of the solid surface will induce free nonzero electric charge densities within the pores of the nanoporous media, which results in the local electric potential field. To figure out the local electric potential within the nanoporous media, the Poisson's equation

$$\nabla^2 \psi = -\frac{\rho_e}{\epsilon_r \epsilon_0}, \quad (14)$$

is solved by a D3Q5 lattice Boltzmann method, which is discussed in details elsewhere (Moran Wang et al., 2006; Yoshida et al., 2014). In Equation (14), ρ_e is defined as $\sum_i e z_i C_i$ and represents the local net electric charge density. The boundary conditions governing the Poisson's equation are $\psi_s(\mathbf{X}) = \psi_{RBL}$, where ψ_{RBL} represents the solid-aqueous solution potential obtained from the RBL model (Alizadeh & Wang, 2018). We note that the RBL model is, in fact, a modification of the electrical triple-layer (ETL) model (Figure 4; Kitamura et al., 1999; Leroy & Revil, 2004; Wang & Revil, 2010). In the RBL model, the local zeta potential is calculated based on the local electro-chemical data for a layer at the vicinity of the solid-aqueous solution interface. In this model, the local chemical reactions of the solid surface with the aqueous solution are considered as



$$\tau_h = \frac{1}{2} + \frac{4\delta_{t,h}}{\delta_x^2} \epsilon_0 \epsilon_r, \quad (9)$$

where δ_x denotes the lattice space, which is equal to 1 in this work. Regarding the equilibrium function, one has (Yoshida et al., 2014)

$$h_i^{\text{eq}} = \omega_i C_i \left(1 + \frac{4\delta_{t,h}}{\delta_x} \left(u - \frac{e z_i D_i}{KT} \frac{\partial \Psi}{\partial x_i} \right) e_i \right), \quad (10)$$

where ω_i are the weight factors as (Yoshida et al., 2014)

$$\omega_i = \begin{cases} \frac{1}{4} & i = 0 \\ \frac{1}{8} & i = 1..6 \end{cases}, \quad (11)$$

and Ψ denotes the total electric potential in space due to both applied external electric field and internal electric field (net free charge density). Finally, the macroscopic amount of the ion concentrations calculates as (Yoshida et al., 2014)

$$C_i(\mathbf{X}, t) = \sum_{i=0}^6 h_i(\mathbf{X}, t). \quad (12)$$

To implement the defined boundary conditions for the ion transport in such a complex geometry like a porous rock, we follow a simple method, which shows that a straightforward bounce-back boundary condition could satisfy the zero ionic fluxes for solid surfaces (Yoshida et al., 2014). Thus, for the unknown distribution functions (h_i) on the solid surfaces, we have (Yoshida et al., 2014)



where K_{a1}^{int} , K_{a2}^{int} , and K_M^{int} represent the associated equilibrium constants for chemical reactions, respectively. We redefined four equations of the ETL's set of equations as

$$K_{a1}^{\text{int}} = \frac{\sigma_{\text{SiOH}}}{\sigma_{\text{SiOH}_2^+}} C_{\text{H}^+,b}^{\text{eff}} \exp\left(-\frac{e\psi_0}{k_B T}\right), \quad (18)$$

$$K_{a2}^{\text{int}} = \frac{\sigma_{\text{SiO}^-}}{\sigma_{\text{SiOH}}} C_{\text{H}^+,b}^{\text{eff}} \exp\left(-\frac{e\psi_0}{k_B T}\right), \quad (19)$$

$$K_M^{\text{int}} = \frac{\sigma_{\text{SiOM}}}{\sigma_{\text{SiO}^-}} \left(\frac{1}{C_{\text{M}^+,b}^{\text{eff}}}\right) \exp\left(\frac{e\psi_\beta}{k_B T}\right), \quad (20)$$

$$Q_d = -\sqrt{8\epsilon_r\epsilon_0 k_B T n_{s,b}^{\text{eff}}} \sinh\left(\frac{e\psi_d}{2k_B T}\right), \quad (21)$$

where

$$n_{s,b}^{\text{eff}} = 1000 N_A \left(C_{\text{M}^+,b}^{\text{eff}} + C_{\text{H}^+,b}^{\text{eff}}\right), \quad (22)$$

denotes the total effective bulk concentration of the counter ions (H^+ and M^+) and Q_d represents the surface charge on the d-plane (the start edge of the diffuse layer). In Equations (18) to (21), the amounts of σ are the surface charge density on the 0 plane. $C_{\text{M}^+,b}^{\text{eff}}$ and $C_{\text{H}^+,b}^{\text{eff}}$ are the effective bulk ion concentration for H^+ and M^+ , which have to be obtained locally for the nanoporous media. The RBL model proposes the effective bulk ion concentration as (Alizadeh & Wang, 2018).

$$C_{\text{H}^+,b}^{\text{eff}} = \begin{cases} \frac{\frac{1}{r_b} \int_0^{r_b} C_{\text{H}^+}(y) dy}{\exp\left(\left(\frac{-e}{k_B T}\right) \psi^{\text{ref}}\right)} \left(\frac{H}{\lambda} = \frac{1}{M}\right) \leq 6 \\ \frac{C_{\text{H}^+}^{r_b}}{\exp\left(\left(\frac{-e}{k_B T}\right) \psi^{r_b}\right)} \left(\frac{H}{\lambda} = \frac{1}{M}\right) > 6 \end{cases}, \quad (23)$$

$$C_{\text{H}^+,b}^{\text{eff}} = \begin{cases} \frac{\frac{1}{r_b} \int_0^{r_b} C_{\text{M}^+}(y) dy}{\exp\left(\left(\frac{-e}{k_B T}\right) \psi^{\text{ref}}\right)} \left(\frac{H}{\lambda} = \frac{1}{M}\right) \leq 6 \\ \frac{C_{\text{M}^+}^{r_b}}{\exp\left(\left(\frac{-e}{k_B T}\right) \psi^{r_b}\right)} \left(\frac{H}{\lambda} = \frac{1}{M}\right) > 6 \end{cases},$$

where

$$\psi_{\text{ref}} = \int_{10^{-6}}^{n_b^m} \frac{\zeta(n_b) dn_b}{n_b^m - 10^{-6}}, \quad (24)$$

denotes the local reference local electric potential, which n_b^m is the bulk ion concentration. In Equation (24), $\zeta(n_b)$ represents the zeta potential of the silica surface for bulk ion concentration (n_b^m), which is simply obtained by solving the set of ETL model's equations. r_b and ψ_{r_b} denote the normal distance from the solid surface to the solution and the local electric potential of the solution at this point, respectively. At the inlet of the nanoporous media, we consider $\psi = 0$ and for the outlet $\partial\psi/\partial x = 0$. In Equation (23), H and M denote the effective pore size of the nanoporous media and the ratio of Debye length to the effective pore size (Zhang & Wang, 2017), respectively.

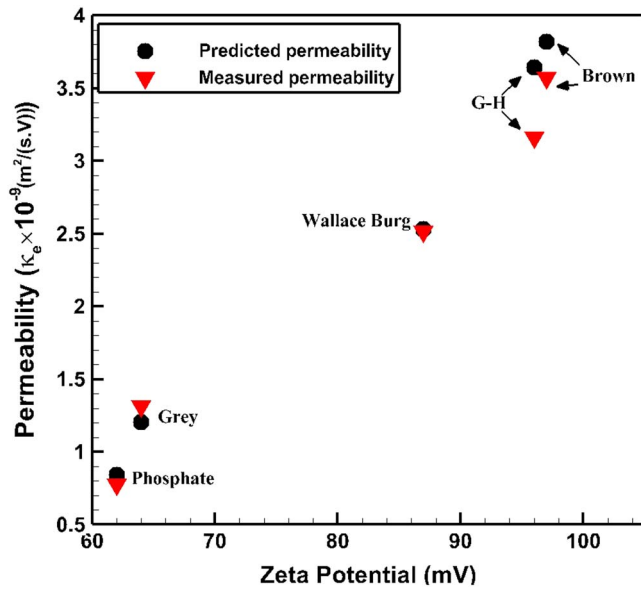


Figure 5. The electroosmotic permeability of different soils (Grey, Phosphate, Wallace Burg, G-H, and Brown; Shang, 1997) compared with the prediction of the present work numerical framework.

To figure out the electroosmotic permeability, we solve the coupled equations Poisson-Nernst-Planck plus Navier–Stokes together with the RBL model to obtain the local surface charge on the randomly generated porous media with the same porosity as the Grey, Phosphate, Wallace Burg, G-H, and Brown soils. Here we should point out that the mineralogical and microstructural properties of the aforementioned solids have not been considered owing to avoid extra complexity for our benchmark. However, our numerical framework could be nicely extended to consider the microstructural and mineralogical specifications of distinct natural soils. In the present work, we utilize the definition of the electroosmotic permeability (Shang, 1997)

$$\kappa_e = \frac{\langle u \rangle_V}{E_p}, \quad (25)$$

where κ_e and $\langle u \rangle_V$ denote the electroosmotic permeability and the average of x -direction fluid flow velocity over the volume of pore spaces, which obtains as $\langle u \rangle_V = (1/V) \int u dV$, at which V denotes the volume of the pore. Later, we will discuss in detail the electroosmotic permeability of the inhomogeneously charged nanoporous media under the overlapped EDLs regime.

In addition to the validation of our numerical framework in complex geometries, we evaluate our numerical framework by comparing the modeling results with the measured electrokinetic conductivity of the nanochannels. To this aim, we solved the PNP + NS equations coupled with the ETL model to obtain the local surface charge on the nanochannel's wall-solution interface. Therefore, one can obtain the streaming current and consequently, the streaming conductance via

$$S_{str} = \frac{1}{\Delta p L} \iint \rho_e(x, y) u(y) dA dx, \quad (26)$$

for the nanofluidic channels which were fabricated by Heyden and co-workers (van der Heyden et al., 2005), where Δp , $u(y)$, and A denote the pressure difference at the inlet and outlet of the nanochannel, the calculated fluid flow velocity, and the cross-section area of the nanochannel, respectively. It is worth noting that the streaming current is a result of applying external electric field, which sweeps up the polarized solution layer formed at the vicinity of a charge solid surface. The accumulation of the counter ions at the low-pressure side of the nanochannel will generate a reverse direction electric field. By measuring this electric field, one can investigate the zeta potential at the solid–liquid interface.

4. Results and Discussion

In this section, first, we will present two benchmarks for evaluating the ion transport phenomena through nanoporous media (soils) and nanofluidic channels with the available experimental results. Afterward, we will investigate the effects of the porosity of the nanoporous media on the electrokinetic transport mechanisms. The electrokinetic conductivity, electroosmotic permeability, and tortuosity would be discussed in details. To exhibit the importance of considering inhomogeneously charged conditions for the nanoporous media, we will compare the prescribed homogeneously charged nanoporous media with the inhomogeneously charged porous media, which obtain their surface charges by considering the local solution properties. All the cases were run on the High-Performance Computing Center of Tsinghua University (Explorer 100).

4.1. Benchmarks

To validate our numerical framework, we employ the available experimental measurements for different soil electroosmotic permeability and nanofluidic channel electrokinetic conductivity. Our modeling results (Figure 5) show good agreement with what was measured by Shang and co-workers (Shang, 1997). However, for G-H and Brown soils the results deviate from the experimental measurements. One main reason in favor of this fact could be the chemical composition of these soils.

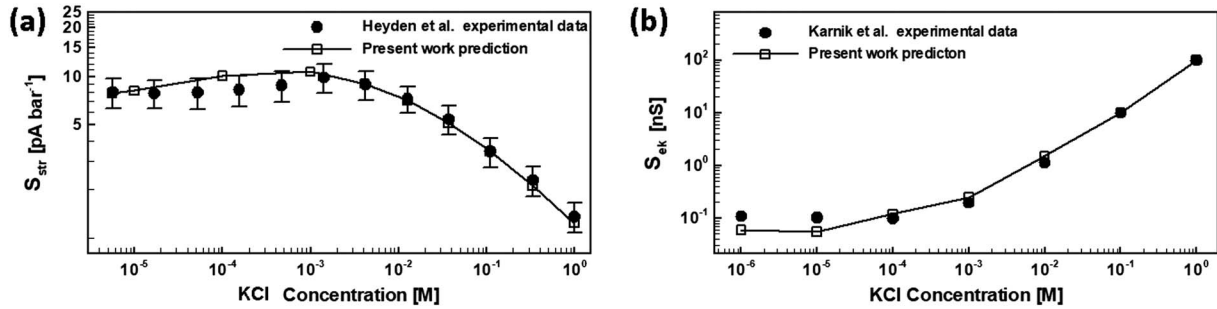


Figure 6. The prediction of the present work numerical framework and comparison with the experimentally measured (a) streaming (height of nanochannel = 70 [nm]; van der Heyden et al., 2005) and (b) electrokinetic (height of nanochannel = 140 [nm]; Karnik et al., 2005) conductance of the nanochannel.

Furthermore, to evaluate our numerical framework for when we apply the external electric field, we solve the governing equations for a nanochannel and figure out the electrical conductance by (Karnik et al., 2005)

$$S_e = \frac{1}{\Delta V L} \sum_i z_i e \int \mathbf{J}_i dA dx, \quad (27)$$

where

$$\mathbf{J}_{i,x} = -\frac{e z_i D_i}{k_B T} C_i \nabla \Psi - D_i \nabla C_i + C_i \mathbf{u}. \quad (28)$$

The electrical conductance through a nanochannel is a result of the ionic fluxes, which migrate due to the applied external electric field.

As Figure 6 illustrates, the present work numerical framework works well in predicting both the streaming and electrical conductivity of the nanochannels for a wide range of bulk ion concentration (10^{-6} to 1 M). It has been shown that for a range of bulk ion concentrations ($n_b < 1 \text{ mM}$), the streaming conductance of the nanochannel is saturated while for electrical conductance this happens for $n_b < 0.01 [\text{mM}]$.

4.2. Porosity Effects on Electrokinetic Transport Phenomena

In order to show the influence of EDL interaction on the electrokinetic transport phenomena, we consider three different randomly generated nanoporous media with distinct porosities (Section 2). By employing the proposed numerical framework in the last sections, Figure 7 depicts slices of 3-D local electric potential (ψ) of the nanoporous media by considering the inhomogeneously acquired charge and the prescribed homogeneous electric charge on the solid-aqueous solution interfaces. The local electric potential is nondimensionalized by the reference zeta potential (ζ_r), which represents the zeta potential obtained by the ETL model (Kitamura et al., 1999; Moran Wang & Revil, 2010) for the reservoir electrolyte solution properties. Modeling results for the nanoporous media with inhomogeneously acquired charge (Figure 7a, 7c, and 7e) show that the absolute value of local electric potential increases in the x direction. As a result, one can conclude that the local electric potential of the porous media mainly varies in the direction of the applied external electric field. In addition, it is revealed that the porosity of the nanoporous media has considerable influence on the averaged local electric potential of the nanoporous media. Figure 7a, 7c, and 7e demonstrate that the nanoporous media with $\varepsilon = 0.6$ and $\varepsilon = 0.3$ has the maximum ($\psi/\zeta_r = 10$) and minimum ($\psi/\zeta_r = 6.2$) local electric potential, respectively. By increasing the porosity, the majority of the pore spaces of the nanoporous media acquire higher local electric potential. This behavior of the local electric potential exhibits an interesting uncovered property of the electric potential distribution within a nanoporous medium in which the pores experience stronger EDL interaction. On the other hand, the homogeneous charge assumption (Figure 7b, 7d, and 7f) shows to what extent there would be a significant difference with inhomogeneously acquired charge scenario. As a matter of fact, prescription of the homogeneously charged nanoporous media restricts our results to have a maximum absolute value of the local electric potential, which is identical to the reference zeta potential. Once more it is worth mentioning that the conventional ETL model cannot predict the surface charge under strong EDL interactions (Alizadeh &

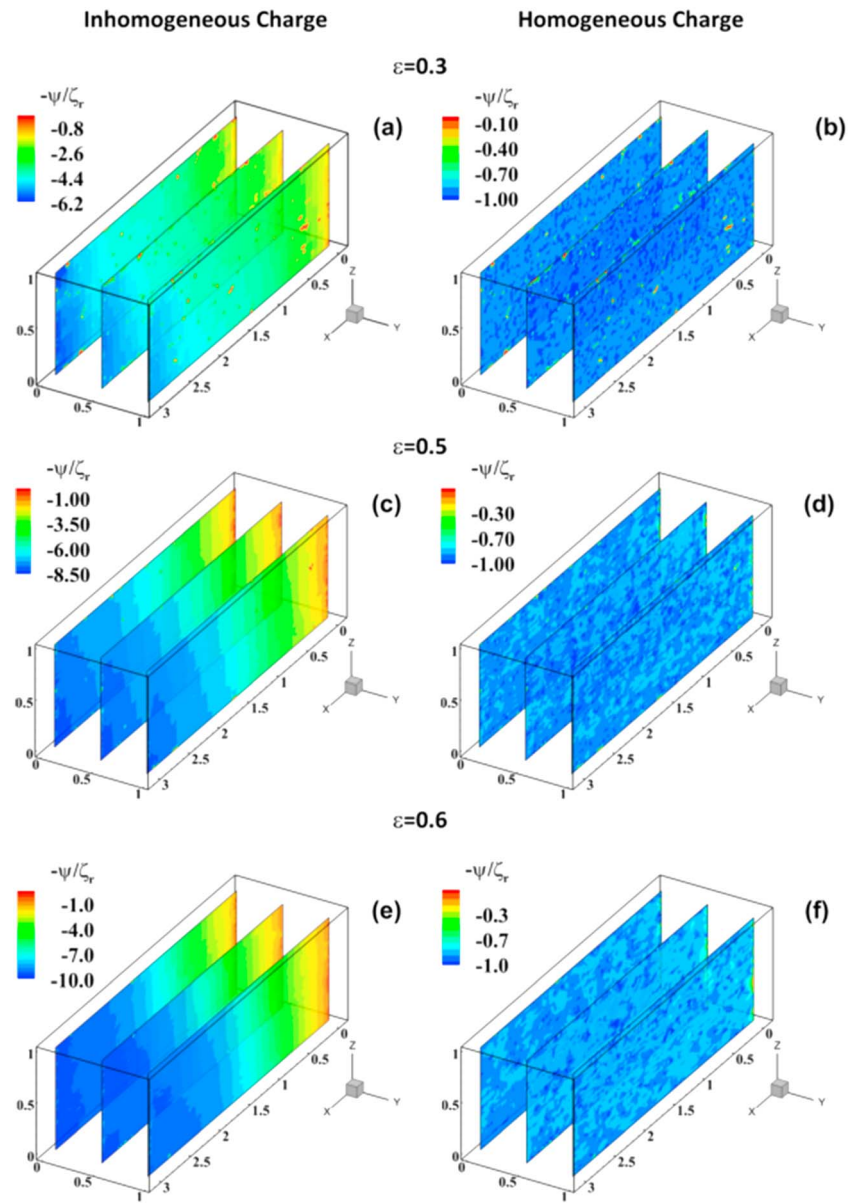


Figure 7. The contour of the dimensionless local electric potential for nanoporous rocks with inhomogeneously acquired surface charge (left column, due to local solution properties) and prescribed homogeneous electric charge (right column, a constant surface charge independent of the local solution properties) with porosities (a and b) $\epsilon = 0.3$, (c and d) $\epsilon = 0.5$, and (e and f) $\epsilon = 0.6$. The porous structures for both homogeneously and inhomogeneously charged scenarios are the same. The local electric potentials are nondimensionalized by the zeta potential for a homogeneous charge, which is obtained by using the ETL model for the reservoir solution properties ($pH = 4$ and $C_{KCl} = 10^{-5}$ [M]) and the x , y , and z axes were nondimensionalized as x/H , y/H , z/H . Both inlet and outlet of the porous media are subjected to the applied external electric field and pressure gradient.

Wang, 2018). For instance, Leroy and Mainault (Philippe Leroy & Mainault, 2018) showed that the linearized Poisson-Boltzmann equation overestimates the electrical potential when the zeta potential is higher than the thermal voltage. As we also expected, this overestimation will be increased when we decrease the salinity. As a result, comparing the inhomogeneous and homogeneous scenarios reveal that by ignoring the EDL interaction and the effects of the local solution properties on the acquired electric charge, there would be more than 83% underestimation for the maximum absolute value of the local electric potential. In simple terms, our modeling results unveil a substantial fact that a nanoporous

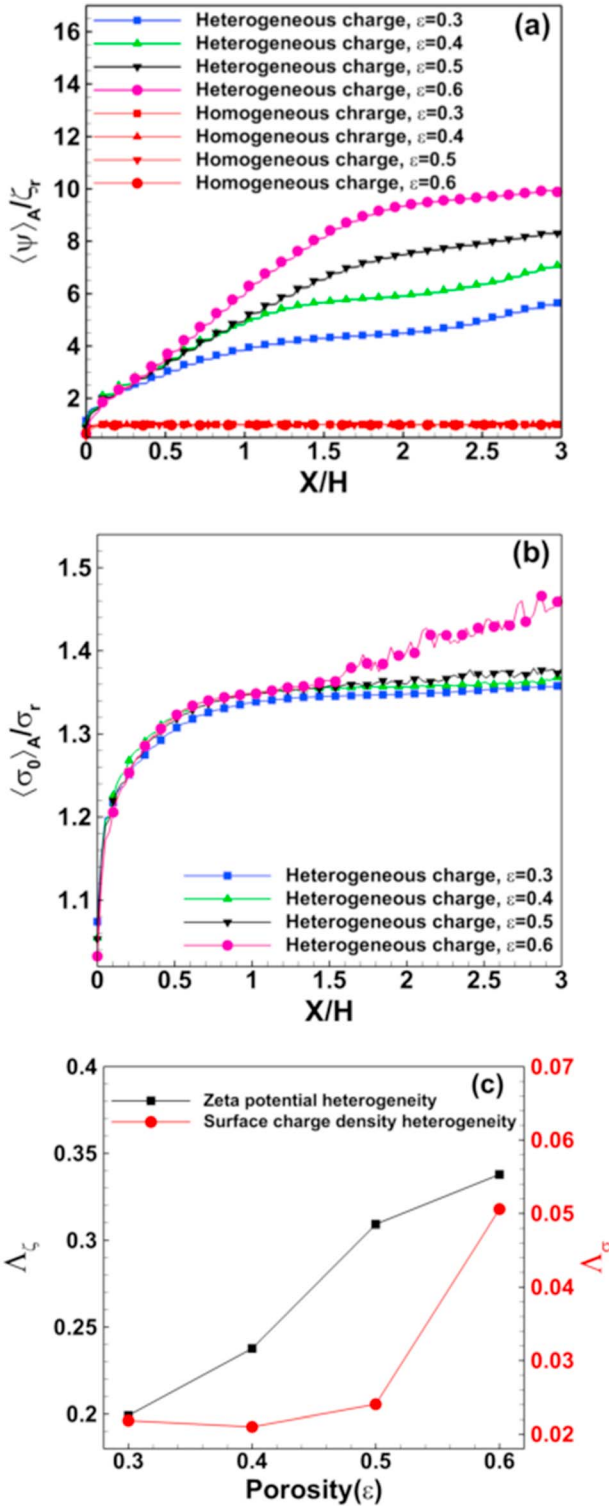


Figure 8. The average of dimensionless (a) local electric potential ($\langle \psi \rangle_A / \zeta_r$) and (b) surface charge density ($\langle \sigma_0 \rangle_A / \sigma_r$) on the yz plane. σ_0 [Cm^{-2}] represents the surface charge density on the 0 plane of the ETL model (Figure 4), and σ_r denotes the surface charge density obtained for the reservoir solution properties. (c) The general inhomogeneity of the zeta potential (Λ_ζ) and surface charge density (Λ_σ) for inhomogeneously acquired charge nanoporous media as a function of porosity.

medium, essentially, acquires higher electric charge compared with the prescribed homogenous surface charge scenario.

To provide a quantitative insight into the distribution of the local electric potential and surface charge density along the x direction of the nanoporous media, we take the average ($\langle \varphi \rangle_A = (1/HW) \int \varphi dy dz$, where φ could be any parameter such as local electric potential, ψ , or surface charge density, σ_0) of the dimensionless local electric potential and surface charge density on the yz -plane (Figure 8a and 8b). As we expected from the contour results (Figure 7), the averaged local electric potential (Figure 8a) increases from inlet to outlet. Moreover, by increasing the porosity of the nanoporous media, the local electric potential generally increases specifically at a distance far from the inlet.

It is interesting to note that from the inlet to $x/H = 0.5$, for inhomogeneously acquired charge nanoporous media, the porosity has not considerably influenced the averaged local electric potential. However, by increasing the distance beyond $x/H = 0.5$, we found that the local electric potential for different porosities increases dramatically and the slope of the increment has direct relationship with the porosity. For the averaged surface charge density ($\langle \sigma_0 \rangle_A$; Figure 8b), similar to that presented for local electric potential, by increasing the distance from the inlet of the nanoporous media, the averaged surface charge density increases. However, in contrast to what we discussed for the local electric potential (Figure 8a), although the surface charge density shows a strong dependence on the distance from the inlet, it does not change significantly when we increase the porosity from 0.3 to 0.5. By increasing the porosity to $\varepsilon = 0.6$, $\langle \sigma_0 \rangle_A$ increases with higher slope than the other porosities. We point that the surface charges of all nanoporous media increase with the same slope when the distance from the inlet is smaller than $x/H = 1.5$. Beyond this distance, the surface charges initiate to increase with different slopes, which have a direct relation with porosity.

In order to investigate the capability of the nanoporous media to induce zeta potential and surface charge inhomogeneity, we define a parameter, Λ , which quantifies the inhomogeneity of the parameter φ as

$$\Lambda_\varphi = \frac{\sum_{i=1}^{k_1} \left| |\varphi(\mathbf{r}_i)| - \frac{\sum_{i=1}^{k_1} |\varphi(\mathbf{r}_i)|}{k_1} \right|}{\sum_{i=1}^{k_1} |\varphi(\mathbf{r}_i)|}, \quad (29)$$

where k_1 and \mathbf{r}_i denote the number of solid-aqueous solution interface nodes in lattice Boltzmann model and the position of that node in (x,y,z) coordinate. By employing the definition of inhomogeneity to quantify the inhomogeneous distribution of the zeta potential (Λ_ζ) and surface charge density (Λ_σ), Figure 8c shows the general inhomogeneity of zeta potential and surface charge density as a function of porosity. Considering Λ_ζ , it is found that by increasing the porosity, the inhomogeneity of zeta potential increases significantly. In contrast to the zeta potential, for the Λ_σ , there would not be a substantial change on the surface charge inhomogeneity when we increase porosity from 0.3 to 0.5. However, the interesting point is that a further increase of the porosity (porosity from 0.5 to 0.6) increases Λ_σ dramatically (more than 50%). This behavior of Λ_σ is expected since the averaged surface charge density showed a higher slope of changes along the nanoporous media for $x/H > 1.5$ when the porosity increases from 0.5 to 0.6 (Figure 8b).

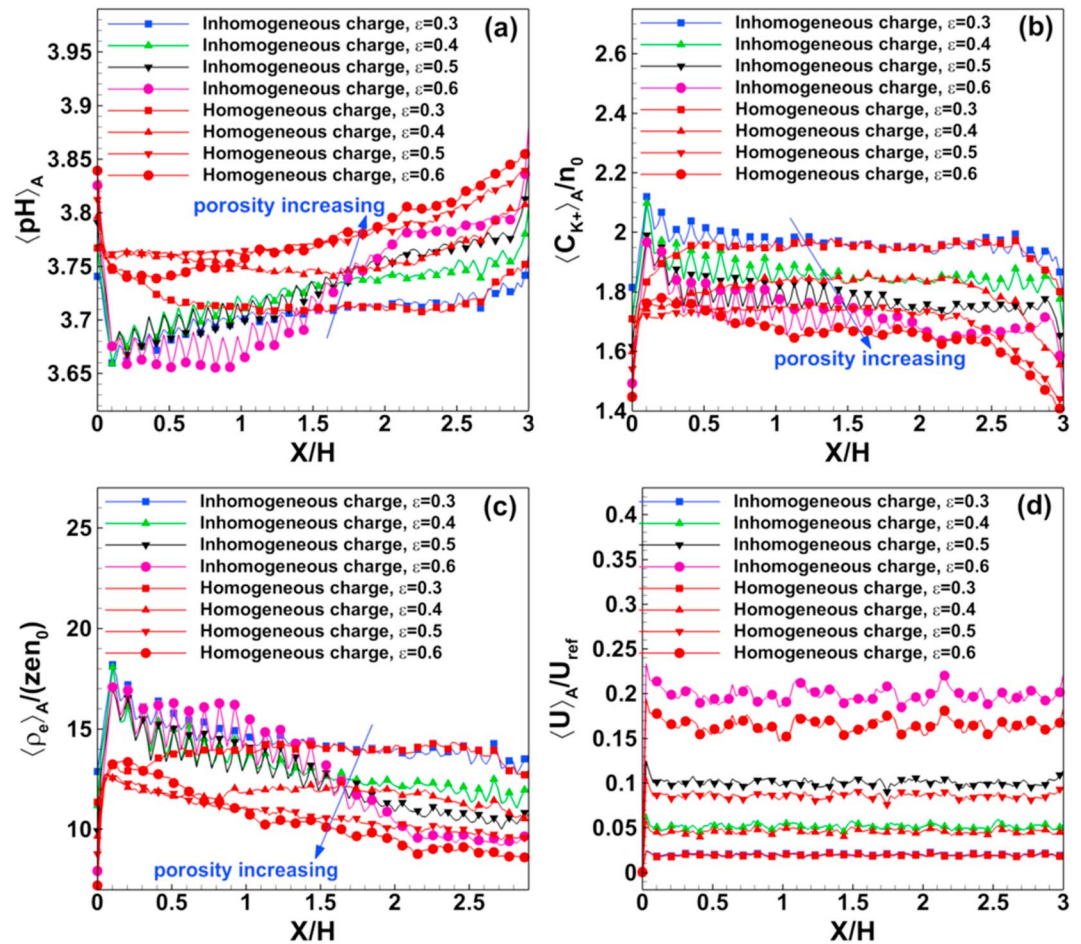


Figure 9. The average of (a) pores solution pH ($\langle pH \rangle_A$), (b) dimensionless K^+ concentration ($\langle C_{K^+} \rangle_A / n_0$), (c) dimensionless net electric charge density ($\langle \rho_e \rangle_A / ze n_0$), and (d) dimensionless solution velocity ($\langle U \rangle_A / U_{ref}$), which is a conclusion of both the pressure gradient and electroosmotic flow velocities along the nanoporous media for inhomogeneously acquired electric charge and homogeneous scenario. The average of the aforementioned amounts is taken over the yz plane of the nanoporous media. Here U_{ref} represents the Helmholtz-Smoluchowski velocity, which was defined in Section 3.

For the increase of Λ_ζ with the porosity, the main reason in favor of this fact is the decreasing of the EDL interactions, which results in decreasing the perm-selectivity of the pores, while the overlapping regime of the EDLs is still retained. This decreasing of the perm-selectivity of the pores results in increasing of inhomogeneity of the surface charge.

Regarding the surface charge and local electric potential of the nanoporous media (Figure 7 and 8), it is essential to interpret the behavior of the nanoporous media when the porosity varies. To this aim, we start from the development of the solution pH and counter-ion concentration along the nanoporous media since they are the two determinative factors to figure out the acquired surface charge on the solid-liquid interfaces. Figure 9a and 9b show the average of solution pH ($\langle pH \rangle_A$) and the dimensionless K^+ concentration $\langle C_{K^+} \rangle_A / n_0$ on the yz plane along the nanoporous media, respectively. As we stated before, by increasing the solution pH, the absolute value of surface charge density and the zeta potential increases. However, the counter-ion concentration (K^+) impacts the surface charge density in contrary to what influenced the zeta potential. By taking into account these two responses of solid-aqueous solution interfaces with silanol groups to solution pH and counter-ion concentration, one can indicate that the main reason of increasing the local electric potential along the nanoporous media (Figure 7 and 8) lies on the ion depletion phenomenon along the nanoporous media. To support this hypothesis, we present Figure 9a, which denotes the variation of $\langle pH \rangle_A$ along the nanoporous media. It is found that the solution pH increases by getting

closer to the outlet and this increment is significantly influenced by the porosity of the nanoporous media. For nanoporous media with porosity $\varepsilon = 0.3$, after a certain distance from the inlet, both homogeneous and inhomogeneous scenarios have identical solution pH. By increasing the porosity, it is revealed that the predicted solution pH for homogeneous charge distribution deviates significantly from that predicted by the inhomogeneous case. Figure 9c shows the nondimensional net electric charge density, which supports the general ion depletion hypothesis along the nanoporous media, whereas the maximum depletion slope is attributed to porosity $\varepsilon = 0.6$. Considering what we have discussed in the present section, one can state the main reason in favor of why increasing the porosity leads to higher absolute values for local electric potential and surface charge density (Figure 8a and 8b). As we know, the acquired surface charge, geometry of the pores, and the solution properties are three coupled factors (Alizadeh & Wang, 2018). Essentially, when we increase the porosity, it means that the interaction of the EDLs would be weaker, while the EDLs are still retained in the overlapped regime. As a result, more co-ions (OH^- and Cl^-) are allowed to enter the pore space. Entering more OH^- results in higher absolute values of surface charges and consequently zeta potentials.

Figure 9d shows the averaged fluid flow velocity ($\langle U \rangle_A / U_{ref}$) along the nanoporous media, which causes due to both applied pressure gradient and the external electric field. It is worth pointing that to obtain a dimensionless velocity, we divide the average cross-sectional velocity by the Helmholtz-Smoluchowski velocity. As it is expected, by increasing the porosity and as a result the mean pore size, the flow velocity increases significantly. It is remarkable to note that the difference in predicted velocity for homogeneous and inhomogeneous surface charge becomes greater by increasing the porosity. The higher zeta potential for inhomogeneous scenario causes higher electroosmotic velocity. In other word, it can be deduced that for a nanoporous medium with $\kappa d_\varepsilon \ll 1$, the surface charge distribution could not affect the fluid flow velocity significantly. The fluctuations of the averaged amounts in Figure 8 and 9 were caused by the inhomogeneous distribution of pore sizes in the nanoporous media.

4.3. Electrokinetic Conductance

Applying the external pressure gradient and electric field results in the ionic fluxes through the nanoporous media. The ions as charge carrying elements would onset electrical current, which is measurable by employing appropriate electrodes at both ends of the nanoporous media. In rocks, the electrokinetic conductance results from transport of the nano-zero net electric charge density, which fill the pores of the porous media (Revil & Glover, 1998). As we mentioned before, in this contribution, we applied both pressure gradient and the external electric field to obtain the streaming potential through the nanoporous rock. Equation (26) demonstrates that the streaming conductance is a function of both net electric charge density and the fluid flow velocity. So by taking into consideration the amounts of κd_ε , which are less than 1.5, one can emphasize that the pore spaces mostly experience nonzero net electric charge density. Therefore, the role of the fluid flow velocity being characteristic to determine the streaming conductance of the nanoporous media. Figure 10a shows the streaming conductance (S_{str}) of the nanoporous media as a function of the porosity for both homogeneous and inhomogeneous surface charge distribution. It is shown that by increasing the porosity, the streaming conductance increases nonlinearly for both surface charge distribution scenarios. To interpret this behavior of streaming conductance, one can address that the net electric charge density decreases (Figure 9c), while the fluid flow velocity increases (Figure 9d). Consequently, the streaming conductance is determined based on the competition of the fluid flow velocity and the net electric charge density. In addition, it is revealed that the homogeneous surface charge predicts streaming conductance with more than 41% underestimation for porosities greater than 0.4.

According to what we mentioned, the ionic fluxes are the outcome of two externally applied pressure and electric field. If we apply an external electric field, the ionic current is obtained by integrating the ionic fluxes (Equation (28)) over the cross section of the nanoporous media (Equation (27)). For a constant applied external electric field, Figure 10b compares the electrical conductance (S_e) for homogeneous and inhomogeneous surface charges. It is shown that the homogeneous surface charge exhibits an increasing electrical conductance with a small slope. On the other hand, for the inhomogeneously acquired surface charge, the electrical conductance dramatically increases by increasing the porous medium porosity. Moreover, the inhomogeneously acquired surface charge predicts at least 73% (e.g., when $\varepsilon = 0.3$) higher amounts of electrical conductance compared with what is predicted by the homogeneous surface charge scenario. The most interesting

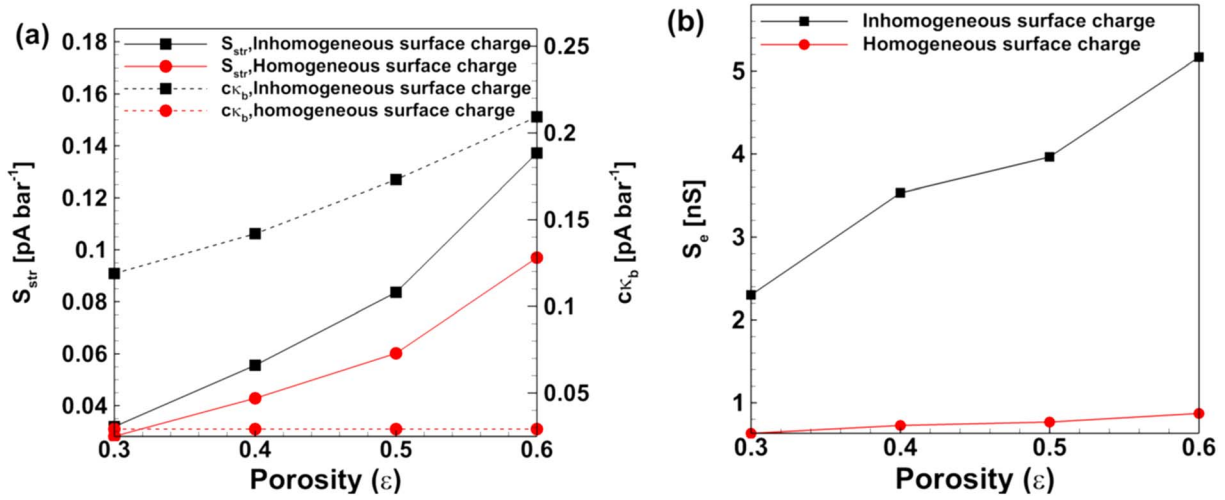


Figure 10. The (a) the streaming conductance (S_{str} [pA bar^{-1}]), which is based on the streaming current measured by the free nonzero net electric charges in the pore spaces and the coupling factor times bulk solution conductivity ($c\kappa_b$ [pA bar^{-1}]), and (b) the electrical conductance (S_e [nS]), which is measured based on the ionic fluxes through the pores, for both homogeneous and inhomogeneous acquired surface charge scenarios.

point is revealed by the response of the electrical conductance of the nanoporous media to porosity when the inhomogeneously acquired surface charge is considered (Figure 10b). Our results unveiled that for porosity $\epsilon < 0.4$ and $\epsilon > 0.5$, the increment of the electrical conductance has higher slope compared with when $0.4 < \epsilon < 0.5$. In other word, our modeling results show that for a different range of porosities, one should not expect the same trend of electrical conductance. To interpret this behavior of the porous media, we need to think of the fact that by increasing the porosity, essentially the role of the pressure-driven part of advection term increases, which results in the increment of the ionic fluxes and consequently the electrokinetic conductance of the porous media. However, as Figure 9d shows, the increment of this velocity with the variation of the porosity would not be with the same rate. One reason in favor of this fact could be due to the effect of the porosity on the electro-osmotic velocity part of the total flow velocity.

Since our modeling results could predict the local zeta potential for the nanoporous media, it is simple to figure out the coupling coefficient (i.e., the ratio of the streaming potential to the applied pressure gradient; Bernabé, 1998) by employing the modified Helmholtz-Smoluchowski equation as (Hunter, 1981)

$$c \equiv \frac{LU}{\Delta p} = -\frac{L\langle\zeta\rangle\epsilon_0\epsilon_r}{\eta\kappa_b}, \quad (30)$$

where $\langle\zeta\rangle$, U , η , and κ_b denote the average of zeta potential over the whole nanoporous media, the streaming potential, the electrolyte viscosity, and the bulk electrolyte conductivity, respectively. Rewriting Equation (30) in the format of

$$c\kappa_b = -\frac{L\langle\zeta\rangle\epsilon_0\epsilon_r}{\eta}, \quad (31)$$

which $c\kappa_b$ has the same dimension as the streaming conductance (A/Pa), we present the $c\kappa_b$ versus porosity in Figure 10a. The interesting point is that the amount of $c\kappa_b$ for inhomogeneously charged nanoporous media is considerably higher than what predicted via the homogeneously charged scenario. A large discrepancy also exists for low porosity in contrast to what we have shown for the streaming conductance.

4.4. Effective Excess Charge Dragged by Water Flow

When the water flows through a charged nanoporous media, the effective excess charge density carries by the water flow could be obtained as (Jougnot et al., 2012)

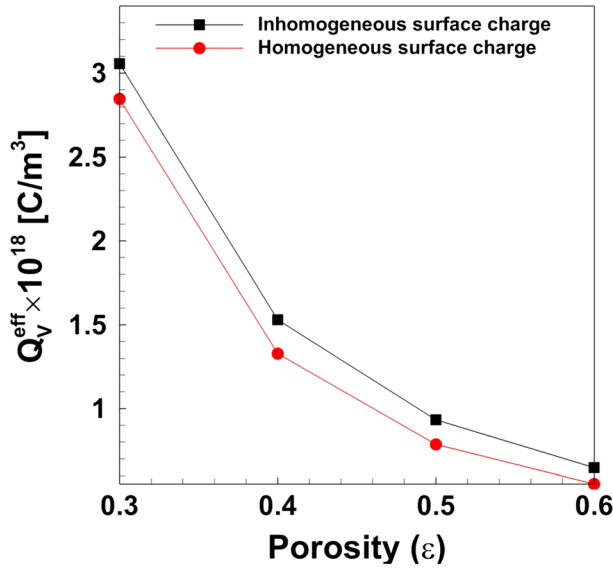


Figure 11. The effective excess charge density versus the porous media porosities for two homogeneously and inhomogeneously charged porous media.

$$Q_V^{\text{eff}} = \frac{1}{\bar{u}V} \int_V \rho_e u dV, \quad (32)$$

where \bar{u} and V represent the average fluid flow velocity in the whole volume of the nanoporous media and the volume of the porous media, respectively. The effective excess charge density is, in fact, what we obtained through the whole porous media. As Guarracino and Jougnot discussed (Guarracino & Jougnot, 2018), the effective excess charge should be distinguished with what we obtained for the pore space. However, in this contribution, we do the integration of the excess charges over the whole pore spaces. Comparing Equation (32) with Equation (26), we will have

$$Q_V^{\text{eff}} = \frac{1}{\bar{u}V} S_{\text{str}} \Delta p L. \quad (33)$$

Equation (33) represents the effective excess charge density for an inhomogeneously charged nanoporous media, which is subjected to an applied pressure gradient. By introducing the streaming conductance (Figure 10a) to Equations (33), Figure 11 demonstrates the effective excess charge densities versus porosities. Our modeling results exhibit a non-linear behavior of the effective excess charge density with the porosity, which would be higher for inhomogeneously charged nanoporous media.

Furthermore, as we also expected, the effective excess charge density is significantly greater for the smaller porosities. However, the slope of the effective excess charge density-porosity curve decreases with porosity, which postulates the fact that for higher porosities, the effective excess charge density will not be significantly changed.

4.5. Electroosmotic Permeability and Tortuosity

The electroosmotic permeability of the nanoporous media is obtained by Equation (25). In addition, J T C Overbeek (1952) proposed a relation for the electroosmotic permeability as

$$\kappa_e = - \frac{\epsilon_r \epsilon_0 \langle \zeta \rangle}{\eta} \left(\frac{K}{K_f} \right), \quad (34)$$

where $\langle \zeta \rangle$ and K/K_f are the average of zeta potential overall solid-aqueous solution interfaces and ratio of the bulk electrolyte conductivity to the nanoporous media conductance, respectively.

One parameter, which is of great interest in studying the transport of the ions and the solution flow through the porous media, is tortuosity. Generally, tortuosity measures the path of the ions or fluid flow through porous media. The physical meaning of tortuosity often changes depending on the problems considered by physicists, engineers, geologists, or other practitioners (Clennell, 1997). For instance, the geometrical tortuosity is the ratio of the shortest path length between two points in the fluid domain over their straight line distance. It is worth pointing out that the geometrical tortuosity is different from what we called hydraulic tortuosity and expressed via Darcy's law. On the other hand, the electrostatic tortuosity is different from the geometrical and hydraulic tortuosity. This tortuosity is related to the ionic exclusion from the pore spaces of a charged porous medium due owing to the presence of the EDLs (Jougnot et al., 2009). According to the definition of the electrostatic tortuosity, it is the ratio between the average concentration of the ionic species in the diffuse layer and the concentration of the ions in the bulk water (Sato et al., 1994), which is defined as

$$\tau_{\text{el}} = \frac{\bar{C}_i}{C_{i,\infty}}, \quad (35)$$

where \bar{C}_i and $C_{i,\infty}$ denote the average of the ionic species in the nanoporous rock and the bulk ion concentration, respectively.

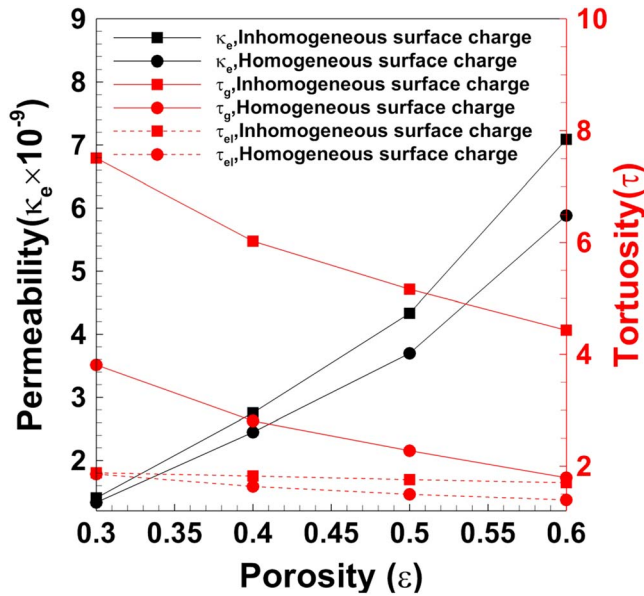


Figure 12. The predicted electroosmotic permeability (κ_e) and tortuosity (τ) as a function of porosity for homogeneously and inhomogeneously acquired charge scenarios.

inhomogeneous charge distributions will predict approximately identical electroosmotic permeability. Moreover, the electroosmotic permeability shows a nonlinear response by increasing the porosity. However, as we expected from a physical point of view, the tortuosity of the nanoporous media should be decreased by increasing the porosity. Figure 12 shows that there is a significant difference between the tortuosity predicted by the homogeneously and inhomogeneously acquired surface charge. The higher tortuosity predicted by the inhomogeneous scenario indicates that the ionic movements in such a nanoporous medium, which the pores acquired inhomogeneous surface charges, would be more tortuous (about 49%) for a prescribed porosity compared with what is predicted by homogeneous charge distribution. Here it is worth noting that the porous structures for inhomogeneous and homogeneous cases are the same. On the other hand, calculating the electrostatic tortuosity for the K^+ indicates that we have higher amounts for inhomogeneous charge cases, which means that for the inhomogeneously charged scenario, the constrictivity of the counter-ions would be greater than the homogeneously charged case.

5. Conclusions

In this work, we conducted a pore-scale study on the ion transport mechanisms through inhomogeneously charged nanoporous rocks. The inhomogeneous charging mechanism took place due to local chemical reactions at the solid-aqueous solution interface. Consequently, the charge inhomogeneity was not a prescribed amount but dependent of the solution properties. To understand the ion transport through nanoporous media with pores screened by the EDLs, we developed a 3-D lattice Boltzmann numerical framework to directly solve the governing equations (PNP + NS). It was shown that prescribing a homogeneous surface charge for the nanoporous media would underestimate the local electric potential significantly. Averaging of the solution properties (e.g., pH, counter-ion concentration, and net electric charge density) over the cross sections of the nanoporous media uncovered a substantial fact that an ion depletion phenomenon would be induced by approaching the outlet of nanoporous media. Our modeling results revealed that for the fully overlapped EDL regime if we increase the porosity of the nanoporous media, the absolute value of acquired surface charge, and consequently the zeta potential would increase. Owing to the effect of porosity and subsequently the interaction of EDLs, we studied the electrical conductance (streaming and electrokinetic) of nanoporous rocks as a function of porosity. Regarding the electrical conductance, the prescribed homogeneous surface charge underestimated the local electric potential about 73% compared with the inhomogeneous scenario. Considering the electroosmotic permeability, we found that the inhomogeneously charged scenario predicted a higher permeability. In addition, we studied the tortuosity of nanoporous

Carman (1956) showed that the electroosmotic permeability can be related to the porosity and tortuosity as

$$\kappa_e = -\frac{\varepsilon \varepsilon_r \varepsilon_0 \langle \zeta \rangle}{\eta \tau_g^2}, \quad (36)$$

where τ_g denotes the geometrical tortuosity. Equation (36) provides a relation to obtaining the geometrical tortuosity as

$$\tau_g = \sqrt{\frac{-\varepsilon \varepsilon_r \varepsilon_0 \langle \zeta \rangle}{\eta \kappa_e}} \quad (37)$$

As Equation (37) represents, the predicted tortuosity is a function of the porous medium structure, the average zeta potential of the solid-aqueous solution interface, and the electroosmotic permeability. However, we note that the geometrical tortuosity is an independent function of the electroosmotic properties.

Figure 12 shows the predicted permeability and tortuosity by the present work numerical framework as a function of porosity. Our modeling results unveiled that by decreasing the porosity, the predicted electroosmotic permeability would be less dependent on the electric charge distribution. In other words, it could be stated that both homogeneous and

rocks for both inhomogeneous and homogeneous surface charge and found that the water flow with local surface charge variation considered was around 49% more tortuous compared to the homogeneous assumption. The present work will improve understanding of the measured data which are collected from underground geological behavior and boost our ability to explain other phenomena like deposition rate of colloids, geological disposal, and protection of radioactive waste, and reactive transport and diffusion transport in clays.

Nomenclature		
Symbol	Description	Unit
ϵ_0	Vacuum electrical permittivity	($\text{CV}^{-1}\text{m}^{-1}$)
ϵ	Porosity	Dimensionless
ϵ_r	Relative permittivity of the solution	Dimensionless
ζ_r	Reference zeta potential	(V)
η	Electrolyte viscosity	(Pa s)
κ	Inverse of Debye length	(m^{-1})
λ	Debye length	(m)
ρ_e	Volume charge density	(Cm^{-3})
σ	Surface charge density	(Cm^{-2})
ϕ	External electric potential	(V)
ψ	Local electric potential	(V)
ω_i	Weight factor	Dimensionless
Ψ	Total electric potential	(V)
C_i	Ionic species concentration	(m^{-3})
c	Coupling coefficient	(VmPa^{-1})
D_i	Ionic species diffusion coefficient	(m^2s^{-1})
e	Electron charge	(C)
E_p	Applied external electric field	(Vm^{-1})
e_i	Discretized lattice velocities	Dimensionless
\mathbf{F}	Body force density	(Nm^{-3})
H	Height of the nanoporous rock	(m)
h_i	Ionic distribution function	Dimensionless
J_i	Ionic fluxes	(m^{-2}s)
L	Length of the nanoporous rock	(m)
$n_{i,0}$	Bulk ionic species concentration	(m^{-3})
p	Applied pressure	(Pa)
Q_V^{eff}	Effective excess charge density	(Cm^{-3})

Acknowledgments

This work is financially supported by the NSF grant of China (51676107 and U1837602), the National Science and Technology Major Project on Oil and Gas (2016ZX05011003), and Tsinghua University Initiative Scientific Research Program. All results presented can be reproduced with the information provided here or can be found in the cited references.

References

- Alizadeh, A., & Wang, M. (2018). Reverse electro dialysis through nanochannels with inhomogeneously charged surfaces and overlapped electric double layers. *Journal of Colloid and Interface Science*, 529, 214–223. <https://doi.org/10.1016/j.jcis.2018.05.111>
- Alizadeh, A., Warkiani, M. E., & Wang, M. (2017). Manipulating electrokinetic conductance of nanofluidic channel by varying inlet pH of solution. *Microfluidics and Nanofluidics*, 21(3), 52. <https://doi.org/10.1007/s10404-017-1892-9>
- Alt-Epping, P., Tournassat, C., Rasouli, P., Steefel, C. I., Mayer, K. U., Jenni, A., et al. (2015). Benchmark reactive transport simulations of a column experiment in compacted bentonite with multispecies diffusion and explicit treatment of electrostatic effects. *Computational Geosciences*, 19(3), 535–550. <https://doi.org/10.1007/s10596-014-9451-x>
- Appelo, C. A. J. (2017). Solute transport solved with the Nernst-Planck equation for concrete pores with 'free' water and a double layer. *Cement and Concrete Research*, 101, 102–113. <https://doi.org/10.1016/j.cemconres.2017.08.030>
- Bernabé, Y. (1998). Streaming potential in heterogeneous networks. *Journal of Geophysical Research*, 103(B9), 20,827–20,841. <https://doi.org/10.1029/98JB02126>
- Bhadra, P., Sengupta, S., Ratchagar, N. P., Achar, B., Chadha, A., & Bhattacharya, E. (2016). Selective transportation of charged ZnO nanoparticles and microorganism dialysis through silicon nanoporous membranes. *Journal of Membrane Science*, 503, 16–24. <https://doi.org/10.1016/j.memsci.2015.12.058>
- Burgreen, D., & Nakache, F. R. (1964). Electrokinetic Flow in Ultrafine Capillary Slits1. *The Journal of Physical Chemistry*, 68(5), 1084–1091. <https://doi.org/10.1021/j100787a019>
- Carman, P. C. (1956). *Flow of gases through porous media*. New York: Academic Press.
- Catalano, J., Lammertink, R. G. H., & Biesheuvel, P. M. (2016). Theory of fluid slip in charged capillary nanopores. arXiv, 8 pp-8 pp.
- Chua, Y. T., Ji, G., Birkett, G., Lin, C. X. C., Kleitz, F., & Smart, S. (2015). Nanoporous organosilica membrane for water desalination: Theoretical study on the water transport. *Journal of Membrane Science*, 482, 56–66. <https://doi.org/10.1016/j.memsci.2015.01.060>
- Clennell, M. B. (1997). Tortuosity: a guide through the maze. *Geological Society, London, Special Publications*, 122(1), 299–344. <https://doi.org/10.1144/gsl.Sp.1997.122.01.18>

- de Lima, S. A., Murad, M. A., Moyne, C., & Stemmelen, D. (2008). A three-scale model for pH-dependent steady flows in 1:1 clays. *Acta Geotechnica*, 3(2), 153. <https://doi.org/10.1007/s11440-008-0070-3>
- Dutta, P., & Beskok, A. (2001). Analytical solution of combined electroosmotic/pressure driven flows in two-dimensional straight channels: Finite Debye Layer Effects. *Analytical Chemistry*, 73(9), 1979–1986. <https://doi.org/10.1021/ac001182i>
- Dykstra, J. E., Keesman, K. J., Biesheuvel, P. M., & van der Wal, A. (2017). Theory of pH changes in water desalination by capacitive deionization. *Water Research*, 119, 178–186. <https://doi.org/10.1016/j.watres.2017.04.039>
- Elimelech, M. (1992). Predicting collision efficiencies of colloidal particles in porous-media. *Water Research*, 26(1), 1–8. [https://doi.org/10.1016/0043-1354\(92\)90104-c](https://doi.org/10.1016/0043-1354(92)90104-c)
- Fair, J. C., & Osterle, J. F. (1971). Reverse electro dialysis in charged capillary membranes. *Journal of Chemical Physics*, 54(8), 3307–3316. <https://doi.org/10.1063/1.1675344>
- Galama, A. H., Post, J. W., Stuart, M. A. C., & Biesheuvel, P. M. (2013). Validity of the Boltzmann equation to describe Donnan equilibrium at the membrane–solution interface. *Journal of Membrane Science*, 442, 131–139. <https://doi.org/10.1016/j.memsci.2013.04.022>
- Gross, R. J., & Osterle, J. F. (1968). Membrane transport characteristic of ultrafine capillaries. *Journal of Chemical Physics*, 49(1), 228–234. <https://doi.org/10.1063/1.1669814>
- Guarracino, L., & Jougnot, D. (2018). A physically based analytical model to describe effective excess charge for streaming potential generation in water saturated porous media. *Journal of Geophysical Research: Solid Earth*, 123, 52–65. <https://doi.org/10.1002/2017JB014873>
- Hotta, K., Yamaguchi, A., & Teramae, N. (2012). Deposition of polyelectrolyte multilayer film on a nanoporous alumina membrane for stable label-free optical biosensing. *The Journal of Physical Chemistry C*, 116(44), 23,533–23,539. <https://doi.org/10.1021/jp308724m>
- Hunter, R. J. (1981). *Zeta Potential In Colloid Science Principles and Applications, BOOK*. New York: Academic Press.
- Johnson, P. R., Sun, N., & Elimelech, M. (1996). Colloid transport in geochemically heterogeneous porous media: Modeling and measurements. *Environmental Science & Technology*, 30(11), 3284–3293. <https://doi.org/10.1021/es960053+>
- Jougnot, D., Linde, N., Revil, A., & Doussan, C. (2012). Derivation of soil-specific streaming potential electrical parameters from hydrodynamic characteristics of partially saturated soils. *Vadose Zone Journal*, 11(1). <https://doi.org/10.2136/vzj2011.0086>
- Jougnot, D., Revil, A., & Leroy, P. (2009). Diffusion of ionic tracers in the Callovo-Oxfordian clay-rock using the Donnan equilibrium model and the formation factor. *Geochimica et Cosmochimica Acta*, 73(10), 2712–2726. <https://doi.org/10.1016/j.gca.2009.01.035>
- Karnik, R., Fan, R., Yue, M., Li, D. Y., Yang, P. D., & Majumdar, A. (2005). Electrostatic control of ions and molecules in nanofluidic transistors. *Nano Letters*, 5(5), 943–948. <https://doi.org/10.1021/nl050493b>
- Kim, D. K., Duan, C. H., Chen, Y. F., & Majumdar, A. (2010). Power generation from concentration gradient by reverse electro dialysis in ion-selective nanochannels. *Microfluidics and Nanofluidics*, 9(6), 1215–1224. <https://doi.org/10.1007/s10404-010-0641-0>
- Kim, S. J., Ko, S. H., Kang, K. H., & Han, J. (2010). Direct seawater desalination by ion concentration polarization. *Nature Nanotechnology*, 5(4), 297–301. <https://doi.org/10.1038/nnano.2010.34>
- Kitamura, A., Fujiwara, K., Yamamoto, T., Nishikawa, S., & Moriyama, H. (1999). Analysis of adsorption behavior of cations onto quartz surface by electrical double-layer model. *Journal of Nuclear Science and Technology*, 36(12), 1167–1175. <https://doi.org/10.3327/jnst.36.1167>
- Ko, S. H., Song, Y.-A., Kim, S. J., Kim, M., Han, J., & Kang, K. H. (2012). Nanofluidic preconcentration device in a straight microchannel using ion concentration polarization. *Lab on a Chip*, 12(21), 4472–4482. <https://doi.org/10.1039/c2lc21238b>
- Kretzschmar, R., Borkovec, M., Grolimund, D., & Elimelech, M. (1999). Mobile subsurface colloids and their role in contaminant transport. In D. L. Sparks (Ed.), *Advances in agronomy* (pp. 121–193). New York: Academic Press. [https://doi.org/10.1016/S0065-2113\(08\)60427-7](https://doi.org/10.1016/S0065-2113(08)60427-7)
- Lacoste, D., Menon, G. I., Bazant, M. Z., & Joanny, J. F. (2009). Electrostatic and electrokinetic contributions to the elastic moduli of a driven membrane. *European Physical Journal E*, 28(3), 243–264. <https://doi.org/10.1140/epje/i2008-10433-1>
- Leroy, P., & Maineult, A. (2018). Exploring the electrical potential inside cylinders beyond the Debye–Hückel approximation: a computer code to solve the Poisson–Boltzmann equation for multivalent electrolytes. *Geophysical Journal International*, 214(1), 58–69. <https://doi.org/10.1093/gji/ggy124>
- Leroy, P., & Revil, A. (2004). A triple-layer model of the surface electrochemical properties of clay minerals. *Journal of Colloid and Interface Science*, 270(2), 371–380. <https://doi.org/10.1016/j.jcis.2003.08.007>
- Li, D. (2004). *Electrokinetics in microfluidics*. Elsevier Academic Press.
- Li, W., Bell, N. A. W., Hernandez-Ainsa, S., Thacker, V. V., Thackray, A. M., Bujdoso, R., & Keyser, U. F. (2013). Single protein molecule detection by glass nanopores. *ACS Nano*, 7(5), 4129–4134. <https://doi.org/10.1021/nn4004567>
- Lichtner, P. C. (1994). Principles and practice of reactive transport modeling. *MRS Proceedings*, 353, 117. <https://doi.org/10.1557/PROC-353-117>
- Liu, X.-B., Chen, Q., Wang, M., Pan, N., & Guo, Z.-Y. (2010). Multi-dimensional effect on optimal network structure for fluid distribution. *Chemical Engineering and Processing-Process Intensification*, 49(10), 1038–1043. <https://doi.org/10.1016/j.cep.2010.07.006>
- Massimo, R., Riccardo, S., Matteo, M., Biao, J., & Muhammad, M. (2018). Nernst-Planck-based Description of transport, Coulombic interactions, and geochemical reactions in porous media: Modeling approach and benchmark Experiments. *Water Resources Research*, 54, 3176–3195. <https://doi.org/10.1002/2017WR022344>
- Molnar, I. L., Johnson, W. P., Gerhard, J. I., Willson, C. S., & O'Carroll, D. M. (2015). Predicting colloid transport through saturated porous media: A critical review. *Water Resources Research*, 51, 6804–6845. <https://doi.org/10.1002/2015WR017318>
- Muhammad, M., & Massimo, R. (2015). Impact of multicomponent ionic transport on pH fronts propagation in saturated porous media. *Water Resources Research*, 51, 6739–6755. <https://doi.org/10.1002/2015WR017134>
- Muhammad, M., & Massimo, R. (2017). Experimental investigation of the impact of compound-specific dispersion and electrostatic interactions on transient transport and solute breakthrough. *Water Resources Research*, 53, 1189–1209. <https://doi.org/10.1002/2016WR019727>
- Muniruzzaman, M., Haberer, C. M., Grathwohl, P., & Rolle, M. (2014). Multicomponent ionic dispersion during transport of electrolytes in heterogeneous porous media: Experiments and model-based interpretation. *Geochimica et Cosmochimica Acta*, 141, 656–669. <https://doi.org/10.1016/j.gca.2014.06.020>
- Muniruzzaman, M., & Rolle, M. (2016). Modeling multicomponent ionic transport in groundwater with IPHreeqc coupling: Electrostatic interactions and geochemical reactions in homogeneous and heterogeneous domains. *Advances in Water Resources*, 98, 1–15. <https://doi.org/10.1016/j.advwatres.2016.10.013>
- Nikonenko, V. V., Kovalenko, A. V., Urtenov, M. K., Pismenskaya, N. D., Han, J., Sistat, P., & Pourcelly, G. (2014). Desalination at over-limiting currents: State-of-the-art and perspectives. *Desalination*, 342, 85–106. <https://doi.org/10.1016/j.desal.2014.01.008>
- Overbeek, J., & Wijga, P. W. O. (1946). On electro-osmosis and streaming-potentials in diaphragms. *Recueil des Travaux Chimiques des Pays-Bas*, 65(8), 556–563. <https://doi.org/10.1002/recl.19460650802>

- Overbeek, J. T. C. (1952). *Colloid Science. Vol. 1. Irreversible Systems*. Amsterdam: Elsevier Publishing Company.
- Peters, P. B., van Roij, R., Bazant, M. Z., & Biesheuvel, P. M. (2016). Analysis of electrolyte transport through charged nanopores. *Physical Review E*, 93(5), 14. <https://doi.org/10.1103/PhysRevE.93.053108>
- Pu, Q. S., Yun, J. S., Temkin, H., & Liu, S. R. (2004). Ion-enrichment and ion-depletion effect of nanochannel structures. *Nano Letters*, 4(6), 1099–1103. <https://doi.org/10.1021/nl0494811>
- Revil, A., & Glover, P. W. J. (1998). Nature of surface electrical conductivity in natural sands, sandstones, and clays. *Geophysical Research Letters*, 25(5), 691–694. <https://doi.org/10.1029/98GL00296>
- Revil, A., & Leroy, P. (2004). Constitutive equations for ionic transport in porous shales. *Journal of Geophysical Research*, 109, B03208. <https://doi.org/10.1029/2003JB002755>
- Revil, A., & Linde, N. (2006). Chemico-electromechanical coupling in microporous media. *Journal of Colloid and Interface Science*, 302(2), 682–694. <https://doi.org/10.1016/j.jcis.2006.06.051>
- Revil, A., Linde, N., Cerepi, A., Jougnot, D., Matthäi, S., & Finsterle, S. (2007). Electrokinetic coupling in unsaturated porous media. *Journal of Colloid and Interface Science*, 313(1), 315–327. <https://doi.org/10.1016/j.jcis.2007.03.037>
- Revil, A., Pezard, P. A., & Glover, P. W. J. (1999). Streaming potential in porous media 1. Theory of the zeta potential. *Journal of Geophysical Research*, 104(B9), 20,021–20,031. <https://doi.org/10.1029/1999JB900089>
- Revil, A., Schwaeger, H., Cathles, L. M., & Manhardt, P. D. (1999). Streaming potential in porous media 2. Theory and application to geothermal systems. *Journal of Geophysical Research*, 104(B9), 20,033–20,048. <https://doi.org/10.1029/1999JB900090>
- Rice, C. L., & Whitehead, R. (1965). Electrokinetic flow in a narrow cylindrical capillary. *The Journal of Physical Chemistry*, 69(11), 4017–4024. <https://doi.org/10.1021/j100895a062>
- Rolle, M., Muniruzzaman, M., Haberer, C. M., & Grathwohl, P. (2013). Coulombic effects in advection-dominated transport of electrolytes in porous media: Multicomponent ionic dispersion. *Geochimica et Cosmochimica Acta*, 120, 195–205. <https://doi.org/10.1016/j.gca.2013.06.031>
- Ryan, J. N., & Elimelech, M. (1996). Colloid mobilization and transport in groundwater. *Colloids and Surfaces A: Physicochemical and Engineering Aspects*, 107, 1–56. [https://doi.org/10.1016/0927-7757\(95\)03384-X](https://doi.org/10.1016/0927-7757(95)03384-X)
- Samson, E., Marchand, J., & Snyder, K. A. (2003). Calculation of ionic diffusion coefficients on the basis of migration test results. *Materials and Structures*, 36(257), 156–165. <https://doi.org/10.1617/14002>
- Sato, H., Yui, M., & Yoshikawa, H. (1994). Diffusion Behavior for Se and Zr in Sodium-Bentonite. *MRS Proceedings*, 353, 269. <https://doi.org/10.1557/PROC-353-269>
- Schultz, D. S. (1997). Electroosmosis technology for soil remediation: Laboratory results, field trial, and economic modeling. *Journal of Hazardous Materials*, 55(1–3), 81–91. [https://doi.org/10.1016/S0304-3894\(97\)00014-9](https://doi.org/10.1016/S0304-3894(97)00014-9)
- Shang, J. Q. (1997). Zeta potential and electroosmotic permeability of clay soils. *Canadian Geotechnical Journal*, 34(4), 627–631. <https://doi.org/10.1139/cgj-34-4-627>
- Song, L. F., Johnson, P. R., & Elimelech, M. (1994). Kinetics of colloid deposition onto heterogeneously charged surfaces in porous-media. *Environmental Science & Technology*, 28(6), 1164–1171. <https://doi.org/10.1021/es00055a030>
- Song, S., Singh, A. K., Shepodd, T. J., & Kirby, B. J. (2004). Microchip dialysis of proteins using in situ photopatterned nanoporous polymer membranes. *Analytical Chemistry*, 76(8), 2367–2373. <https://doi.org/10.1021/ac035290r>
- Steeffel, C. I., & Maher, K. (2009). Fluid-rock interaction: A reactive transport approach. In E. H. Oelkers & J. Schott (Eds.), *Thermodynamics and Kinetics of Water-Rock Interaction*, *GeoScience World* (pp. 485–532). <https://doi.org/10.2138/rmg.2009.70.11>
- Sun, N., Elimelech, M., Sun, N. Z., & Ryan, J. N. (2001). A novel two-dimensional model for colloid transport in physically and geochemically heterogeneous porous media. *Journal of Contaminant Hydrology*, 49(3–4), 173–199. [https://doi.org/10.1016/S0169-7722\(00\)00193-5](https://doi.org/10.1016/S0169-7722(00)00193-5)
- Sung Jae, K., Hee, K. S., Hyoung, K. K., & Jongyoon, H. (2010). Direct seawater desalination by ion concentration polarization. *Nature Nanotechnology*, 5(4), 297–301. <https://doi.org/10.1038/nnano.2010.34>
- Suss, M. E., Baumann, T. F., Bourcier, W. L., Spadaccini, C. M., Rose, K. A., Santiago, J. G., & Stadermann, M. (2012). Capacitive desalination with flow-through electrodes. *Energy & Environmental Science*, 5(11), 9511–9519. <https://doi.org/10.1039/C2EE21498A>
- Tobiason, J. E. (1989). Chemical effects on the deposition of non-brownian particles. *Colloids and Surfaces*, 39(1–3), 53–77. [https://doi.org/10.1016/0166-6622\(89\)80178-7](https://doi.org/10.1016/0166-6622(89)80178-7)
- van der Heyden, F. H. J., Stein, D., & Dekker, C. (2005). Streaming currents in a single nanofluidic channel. *Physical Review Letters*, 95(11), 4. <https://doi.org/10.1103/PhysRevLett.95.116104>
- Vane, L. M., & Zang, G. M. (1997). Effect of aqueous phase properties on clay particle zeta potential and electro-osmotic permeability: Implications for electro-kinetic soil remediation processes. *Journal of Hazardous Materials*, 55(1–3), 1–22. [https://doi.org/10.1016/S0304-3894\(97\)00010-1](https://doi.org/10.1016/S0304-3894(97)00010-1)
- Wang, M., & Chen, S. (2007). Electroosmosis in homogeneously charged micro- and nanoscale random porous media. *Journal of Colloid and Interface Science*, 314(1), 264–273. <https://doi.org/10.1016/j.jcis.2007.05.043>
- Wang, M., & Kang, Q. (2010). Modeling electrokinetic flows in microchannels using coupled lattice Boltzmann methods. *Journal of Computational Physics*, 229(3), 728–744. <https://doi.org/10.1016/j.jcp.2009.10.006>
- Wang, M., Kang, Q., & Ben-Naim, E. (2010). Modeling of electrokinetic transport in silica nanofluidic channels. *Analytica Chimica Acta*, 664(2), 158–164. <https://doi.org/10.1016/j.aca.2010.02.018>
- Wang, M., Kang, Q., Viswanathan, H., & Robinson, B. A. (2010). Modeling of electro-osmosis of dilute electrolyte solutions in silica microporous media. *Journal of Geophysical Research*, 115, B10205. <https://doi.org/10.1029/2010JB007460>
- Wang, M., & Revil, A. (2010). Electrochemical charge of silica surfaces at high ionic strength in narrow channels. *Journal of Colloid and Interface Science*, 343(1), 381–386. <https://doi.org/10.1016/j.jcis.2009.11.039>
- Wang, M., Wang, J., Chen, S., & Pan, N. (2006). Electrokinetic pumping effects of charged porous media in microchannels using the lattice Poisson-Boltzmann method. *Journal of Colloid and Interface Science*, 304(1), 246–253. <https://doi.org/10.1016/j.jcis.2006.08.050>
- Wang, M., Wang, J., Pan, N., Chen, S., & He, J. (2007). Three-dimensional effect on the effective thermal conductivity of porous media. *Journal of Physics D-Applied Physics*, 40(1), 260–265. <https://doi.org/10.1088/0022-3727/40/1/024>
- Yang, Y., & Wang, M. (2018a). Pore-scale modeling of chloride ion diffusion in cement microstructures. *Cement and Concrete Composites*, 85, 92–104. <https://doi.org/10.1016/j.cemconcomp.2017.09.014>
- Yang, Y., & Wang, M. (2018b). Pore-scale study of thermal effects on ion diffusion in clay with inhomogeneous surface charge. *Journal of Colloid and Interface Science*, 514, 443–451. <https://doi.org/10.1016/j.jcis.2017.12.047>
- Yanuka, M., Dullien, F. A. L., & Elrick, D. E. (1986). Percolation processes and porous media. *Journal of Colloid and Interface Science*, 112(1), 24–41. [https://doi.org/10.1016/0021-9797\(86\)90066-4](https://doi.org/10.1016/0021-9797(86)90066-4)

- Yoshida, H., Kinjo, T., & Washizu, H. (2014). Coupled lattice Boltzmann method for simulating electrokinetic flows: A localized scheme for the Nernst-Planck model. *Communications in Nonlinear Science and Numerical Simulation*, *19*(10), 3570–3590. <https://doi.org/10.1016/j.cnsns.2014.03.005>
- Zhang, L., & Wang, M. (2015). Modeling of electrokinetic reactive transport in micropore using a coupled lattice Boltzmann method. *Journal of Geophysical Research: Solid Earth*, *120*, 2877–2890. <https://doi.org/10.1002/2014JB011812>
- Zhang, L., & Wang, M. (2017). Electro-osmosis in inhomogeneously charged microporous media by pore-scale modeling. *Journal of Colloid and Interface Science*, *486*, 219–231. <https://doi.org/10.1016/j.jcis.2016.09.057>